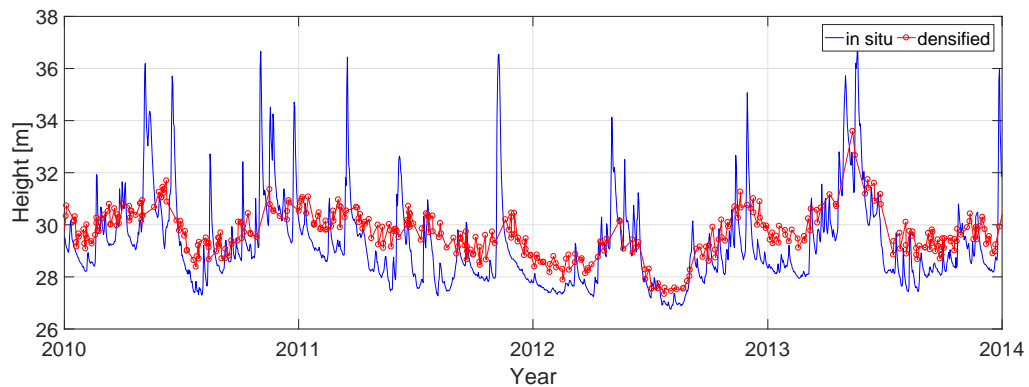


Assessment of Altimetric River Water Level Time Series Densification Methods



Master Thesis
Geodesy and Geoinformation
University of Stuttgart

Zhuge Xia

Stuttgart, Germany, September 2018

Supervisor: Dr. Hassan Hashemi Farahani
University of Stuttgart

Prof. Dr. -Ing. Nico Sneeuw
University of Stuttgart

Erklärung der Urheberschaft

Ich erkläre hiermit an Eides statt, dass ich die vorliegende Arbeit ohne Hilfe Dritter und ohne Benutzung anderer als der angegebenen Hilfsmittel angefertigt habe; die aus fremden Quellen direkt oder indirekt übernommenen Gedanken sind als solche kenntlich gemacht. Die Arbeit wurde bisher in gleicher oder ähnlicher Form in keiner anderen Prüfungsbehörde vorgelegt und auch noch nicht veröffentlicht.

Ort, Datum

Unterschrift

Abstract

Nowadays, collecting and analysing water level time series recorded by gauging stations or by satellite altimetry is crucial for the geodetic and environmental purposes, such as modelling ocean circulation and monitoring climate change. Since the 1970s, a large number of gauging stations has been removed. This has made altimetry increasing more important. However, data collected by individual altimetric satellites are limited, i.e., the temporal resolution is limited to the repeat cycle of satellites, and the spatial resolution is constrained to the distribution of virtual stations. In order to overcome these limitations, methods have been developed to combine all available altimetric satellite missions along a river to construct a new densified time series. This is referred to as densification. To our knowledge, there are only two proven densification methods applied to the river for now. The first is a hydraulic statistic densification method developed by Tourian et al. (2016). The other is the kriging densification method published by Boergens et al. (2017). However, each of them is realized under different circumstances, which makes them incomparable with each other. In this work, we implement the two densification methods and apply them under similar conditions. The various densified water level time series are compared and analysed both visually and statistically. Results reveal different characteristics of the two densification methods.

Contents

Declaration	III
Abstract	VIII
1 Introduction	1
1.1 Background	1
1.2 Previous Studies and Motivation	3
1.2.1 Development History of Densification	3
1.2.2 Proven Densification Technique	4
1.2.3 Comparison Strategy	5
1.3 Outline	6
2 Data and Survey Specifications	7
2.1 Combination of Satellite Missions	7
2.1.1 TOPEX/Poseidon and TOPEX Extended Mission ²	7
2.1.2 ENVISAT and ENVISAT Extended Mission ³	7
2.1.3 OSTM/JASON-2 ⁴	8
2.1.4 SARAL/ALTIKA ⁵	8
2.1.5 Resolution and Duration for Satellite Missions	8
2.2 Survey Area and River	9
2.3 Gauging Stations	10
2.4 Virtual Stations	11
3 Methodology	15
3.1 Hydraulic Statistic Densification Method	15
3.1.1 Overview of Densification Procedure	15
3.1.2 Estimation of Parameters and River Velocity Model	16
3.1.3 Estimation of Time Lag between Virtual Stations	20
3.1.4 Combination of Altimetric Time Series and Reconstruction	21
3.2 Kriging Densification Method	22
3.2.1 Introduction of Ordinary Kriging	22
3.2.2 Overview of Densification Procedure	24
3.2.3 Estimation of Residual Time Series of River Water Level	24
3.2.4 Estimation of Spatio-temporal Covariance Model	25
3.2.5 Estimation of Weights and Consequent Predicted Water Level Time Series	31
3.2.6 Restore and Combination	32

3.3	Non-linear Least Squares Estimation	32
3.4	Data Snooping Method	33
3.5	Interpolation Method	35
4	Comparison and Analysis	37
4.1	Comparison of Densification Methods	37
4.1.1	Similarities	37
4.1.2	Differences	38
4.2	Validation of Hydraulic Statistic Densification Method	38
4.3	Validation of Kriging Densification Method	41
4.4	Specific Graphical Comparison	43
4.4.1	Case 1	43
4.4.2	Case 2	44
4.4.3	Case 3	45
4.5	General Numerical Comparison of the Densification Methods	46
5	Conclusion and Outlook	51
5.1	Conclusion	51
5.2	Outlook	54
	Bibliography	XVI
	A Anhang	XVII
	B Anhang	XIX

List of Figures

1.1	Altimetry principle ¹	2
2.1	Po river from river source to mouth ⁶	9
2.2	Distribution of gauging stations and virtual stations along the Po river.	10
2.3	Synoptic visualization of water level time series at all virtual stations between 1992 and 2018.	12
3.1	Variations of (a) river discharge, (b) river flow velocity, (c) river width, and (d) river slope at four gauging stations Cremona, Borgoforte, Sermede and Pontelagoscuro between 2002 and 2011.	17
3.2	Relative root-mean-squared errors of flow velocity models at four gauging stations <i>Cremona, Borgoforte, Sermede</i> and <i>Pontelagoscuro</i> . Errors are: (a) 20.55%, (b) 20.37%, (c) 26.39%, (d) 35.33%. RMS of real flow velocity are: (a) 6.79, (b) 7.00, (c) 4.96, (d) 6.75. RMS of residual data are: (a) 3.21, (b) 4.49, (c) 3.74, (d) 4.21. The red lines reveal the real velocities at the gauging stations. The blue lines reveal the predicted velocities.	19
3.3	Time lags of virtual stations along the Po river. Crosses here are referred to as the defined 43 virtual stations along the river.	21
3.4	Example of observation transformation to residual time series (Jason-2). The black line represents the original time series of water level. The blue line is the mean value. The green line reveals the seasonal variations of the Po river. The red line is the residual time series.	25
3.5	Empirical covariance models and the corresponding fittings in time and space.	30
3.6	Example of data snooping at the gauging station Piacenza between 1995 and 2005. The blue points are the densified time series of water level. The two red lines are the upper and lower limitations of the confidence intervals for every iteration. The two black lines are the final interval limitations.	33
3.7	Zoomed-in figure for details display between 2008 and 2012. The blue points are the densified time series of water level. The two red lines are the upper and lower limitations of the confidence intervals for every iteration. The two black lines are the final interval limitations.	35

3.8	The zoomed-in densified time series as well as interpolated data against daily in situ at gauging station Piacenza in year 2007. The red line is the original densified water level time series. The blue line is the in situ data at gauging station. The green one is the interpolated densified time series with cubic interpolation.	36
4.1	Hydraulic statistic method densified water level time series against in situ data at five gauging stations: (a) Piacenza, (b) Cremona, (c) Borgoforte, (d) Sermide, (e) Pontelagoscuro between 1995 and 2014. The red line shows the densified water level time series. The blue line is the in situ data.	39
4.2	Kriging method densified water level time series against in situ data at five gauging stations: (a) Piacenza, (b) Cremona, (c) Borgoforte, (d) Sermide, (e) Pontelagoscuro between 1995 and 2014. The red line shows the densified water level time series. The blue line is the in situ data.	41
4.3	First example of detailed comparison at second gauging station Cremona between 2010 and 2014. The red line shows the densified water level time series. The blue line is the in situ data.	43
4.4	Second example of detailed comparison at third gauging station Borgoforte between 2000 and 2004. The red line shows the densified water level time series. The blue line is the in situ data.	44
4.5	Third example of detailed comparison at fifth gauging station Pontelagoscuro between 2004 and 2009. The red line shows the densified water level time series. The blue line is the in situ data.	45

List of Tables

2.1	Combination of different satellite data sets.	9
2.2	Information about Po river ⁷	10
2.3	Latitude, longitude, and mean water level at gauging stations along the Po river.	11
2.4	List for defined virtual stations along the Po river.	13
2.5	List for defined virtual stations along the Po river (Continuation of Table 2.4).	14
3.1	Random example of parameters of covariance functions. m is the order of observations. s is the distance from the river source. t is the data observing time. Z is the residual time series of water level.	27
3.2	Parameters of the fitting model.	30
3.3	Accuracies of satellite missions ⁸	32
4.1	Statistics (m) of differences between time series densified based on the hydraulic statistic densification method and in situ data at five gauging stations.	39
4.2	Statistics (m) of differences between time series densified based on the kriging densification method and in situ data at five gauging stations.	42
4.3	Numerical comparisons between hydraulic statistic densification method and the kriging densification method. Green data suggest a better performance using the kriging densification method. Red data refer to as worse results for the kriging method. Also, HSD = hydraulic statistic densification and KD = kriging densification.	46
5.1	Improvements in percentage using the kriging densification method against the hydraulic statistic densification method. Green data suggest a better performance using the kriging densification method. Red data refer to as worse results for the kriging method.	52
A.1	Influence of CryoSat-2 mission for the hydraulic statistic densification method. (NW = data without CryoSat-2, W = data with CryoSat-2.)	XVII
B.1	Influence of applying residual time series for the hydraulic statistic densification method. (ALL = applying total data, RES = applying residual data.)	XIX

Chapter 1

Introduction

1.1 Background

In recent years, the radar altimetry technique based on airborne platforms or satellites has been widely used for hydrological applications. Satellite altimetry was designed initially for oceanography. After decades of continuous improvements, it can now be applied to obtain and investigate water height variations at unique geographical locations in a lake or along a river. Among these inland water resources, some special locations are identified as virtual stations, where the projections of satellite tracks on the ground cross those water bodies. Time series of water level could be derived at such virtual stations. In this work, we use data collected at such locations. This section provides the background of satellite altimetry, its measurement principle as well as its contributions.

The measurement principle in radar altimetry is to acquire the travel time of a pulse sent from altimeter to the water surface and then received back by the satellite (Tourian, 2012). After signal corrections and waveform analysis (i.e., retracking), it is possible to obtain the water level height. As shown below:

$$SSH = S - R. \quad (1.1)$$

Herein, SSH is the sea surface height, which is the range at a given instant from the sea surface to a reference ellipsoid. S is the altitude of the satellite relative to the same reference surface. Positioning systems such as Global Navigation Satellite System (GNSS) and Doppler Orbitography and Radiopositioning Integrated by Satellite (DORIS) yield the satellite's position with a high accuracy. Herein, R is the distance from satellite to water surface, which can be estimated by measuring the travel time t of the emitted echo:

$$R = \frac{1}{2} \cdot c \cdot t. \quad (1.2)$$

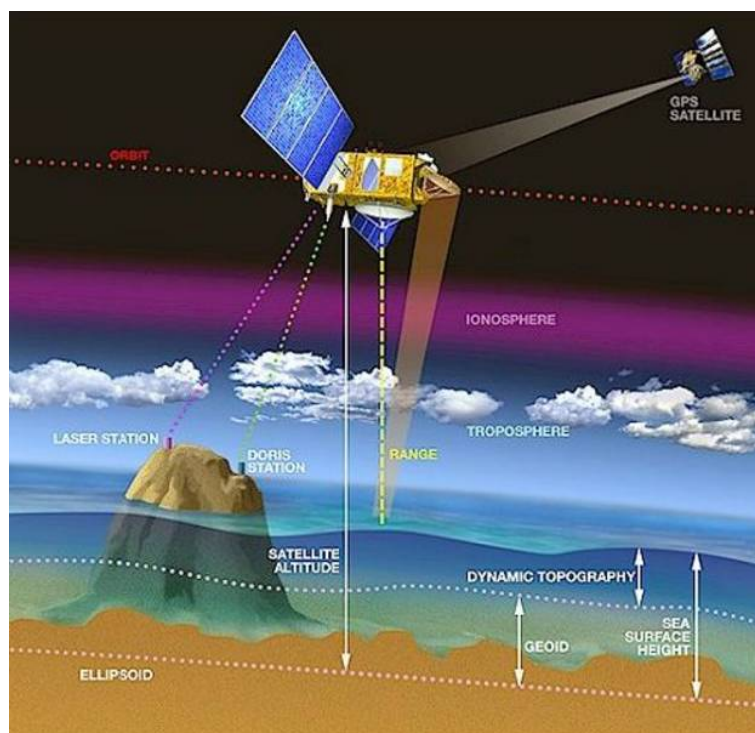


Figure 1.1: Altimetry principle¹.

Thanks to satellite altimetry technique, we can better understand geodetic and environmental aspects of the Earth. Numerous applications can be fulfilled. Examples are:

- (i) To continuously observe the sea surface topography. Similar to the land topography, the ocean surface has highs and lows as well. These variations are referred to sea surface topography.
- (ii) To determine ocean currents and circulations as well as other ocean features.
- (iii) To produce a global tidal map.
- (iv) To determine the Earth's gravity field.
- (v) To estimate sea surface temperature.

However, according to Alsdorf et al. (2007), our knowledge about the spatio-temporal distributions and variations of surface fresh water on the Earth is still quite limited in many hydrological applications. Hence, measuring and analysing the water surface height time series by gauging stations or by independent sensors from satellite altimetry is a vitally important work. Processing altimetric data allow us to acquire relationships and interactions of water bodies, and to simulate and describe the hydrological pattern at the global scale. However, given the fact that a large quantity of gauging stations is reduced since the 1970s (Milzow et al., 2011), the independent altimetric

¹<https://www.aviso.altimetry.fr/en/techniques/altimetry/principle/basic-principle.html>.

missions could play a more critical role to fill the gaps caused by the declining gauging stations. Furthermore, one could safely assume that most of the gauging stations would be replaced by satellite altimetry anyway in the future. To achieve such a goal, there are still many steps involving many challenges, e.g., the time series produced by single altimetry are subject to multiple limitations.

On the one hand, the related temporal resolution by single altimetry is relatively too long compared to the standard daily in situ data collected by gauging stations. The reason is that the temporal resolution by single altimetry is limited due to the repeat cycle of satellite, e.g., ten days for TOPEX/Poseidon, TOPEX extended mission and JASON series, or 35 days for ENVISAT, ENVISAT extended mission and SARAL/ALTIKA. On the other hand, the spatial resolution is also constrained due to the related ground track pattern and the distribution of virtual stations. These limitations stimulate developments of methods to combine data from multiple missions and produce densified data. This procedure is referred to as densification.

1.2 Previous Studies and Motivation

1.2.1 Development History of Densification

For decades, satellite altimetry has shown its capability of surface height measurements with high accuracies for water bodies. At the beginning, suggested by Birkett (1995), the accuracy of satellite altimetry to determine the water level height of inland water bodies could only reach dm-level. After numerous improvements, such as advanced retracking techniques, we can now achieve cm-level accuracy (Tourian et al., 2016). For example, the accuracy of CryoSat mission is excellent and could reach 1–3 cm for inland applications (Nielsen et al., 2015).

However, these high-accuracy river water level data at virtual stations are only produced by single altimeter, resulting in limitations mentioned in the previous section. In the last few years, researchers have combined different altimetric missions to conduct water level analysis and to overcome those limitations. For example, the concept of the combination was advocated for the first time over multiple lakes to deal with the problem of low altimetric temporal resolution by Crétaux and Birkett (2006). In that study, an assumption was made that the lake surface is logically equipotential. Because the water level above the geoid should remain steady when there are no exterior effects such as wind or current. That is the basis why different altimetric missions could be joint together and a combination of multi-satellite missions into single time series could be realized.

After the successful combination of multi-satellite over lakes, geodesists started to extend this approach to other water bodies, which is significant to fill the gap caused by the declining gauging stations. According to Tourian et al. (2016), the database in the hydrological field (such as discharge) is more available in public to a certain extent

than the gauging station in situ data of water level. This encourages an expansion of the combination from lakes to rivers. However, combining altimetric missions along rivers is entirely different from lakes. There are some possible reasons:

- (i) There is no similar equipotential surface for a river. Its altitude is changing with the topography.
- (ii) The river is floating so that the corresponding structure is dynamic and the combination of missions is hindered. In other words, the slope and flow velocity of the river could change greatly and rapidly, increasing the difficulty to simulate the prediction model.
- (iii) The distribution of virtual stations could cover the river unevenly, which makes the scattered locations with altimetric data disproportional, i.e., some river areas may possess denser information than the others.

To solve these problems and obtain water level time series along a river, research efforts has been made. For the first time, Birkinshaw et al. (2010) conducted an examination of the Mekong river by combining all the altimetry data within the same period, though regardless their time lags between virtual stations. Besides, the combined data are not fully employed because the outlier-free altimetric data over the Mekong are only used to improve the quality of velocity estimation.

Then a further demonstration was made by Michailovsky et al. (2013) to apply with an approach by deriving an altimetric water level into hydrological river model using so-called assimilation method.

Besides, after four years, Birkinshaw et al. (2014) proposed a method to calculate the daily quantity of flow at an unmeasured station using ENVISAT altimetry and LANDSAT images. However, in their approach, there is no indication of water travel time and biases between satellite missions.

More recent studies by Tourian et al. (2016) and Boergens et al. (2017) have achieved the goal to produce densified time series along rivers.

1.2.2 Proven Densification Technique

To our knowledge, there are only two different densification methods over rivers that have been maturely developed so far.

- (i) The first method, published by Tourian et al. (2016) from the University of Stuttgart, is a hydraulic statics densification method based on the estimation of river flow velocity and the time lag between virtual stations. The methods was applied over the Po river.

- (ii) The second method is a kriging densification method proposed by Boergens et al. (2017) from the Technical University of Munich. This approach is based on the ordinary kriging method – an interpolation method for spatial data, and the covariance model to connect the observations. They applied their approach along the Mekong river.

Chapter 3 will display the detailed explanations about the processing for these two densification methods.

Note that these two methods were applied under different circumstances, e.g., different combinations of satellite missions, two different rivers, different gauging stations and virtual stations along the rivers. These differences make these methods incomparable with each other. Therefore, the question arises that which one of these two densification methods is of a better performance and what their characteristics are. This thesis aims to implement these two densification methods under the same circumstances. The same river is chosen. The same combination of missions is chosen. And, the same gauging data are used for validation. This makes the comparison between the two methods feasible. The outcome of the work is valuable, because it allows for a fair comparison of the two methods.

1.2.3 Comparison Strategy

This section describes the proper comparison strategies between two densification methods so that an analogous and fair circumstance for valid comparison is created.

- (i) The same river should be applied. In this work the Po river in Northern Italy – the same river that Tourian et al. (2016) used.
- (ii) The same set of virtual stations along the river should be applied. Over the Po river, there are generally 43 virtual stations.
- (iii) The same in situ data at gauging stations along the river for validation should be applied. Over Po river, there are five gauging stations, i.e., Piacenza, Cremona, Borgoforte, Sermide and Pontelagoscuro from river source to river mouth.
- (iv) The same combination of altimetric satellite missions should be used. There is generally six satellite mission for the combination, i.e., TOPEX, TOPEX extended, ENVISAT, ENVISAT extended, SARAL and JASON-2.
- (v) The same processing technique should be used, e.g., non-linear least squares estimation for calculating modelling parameters and data snooping method to remove the outliers from the densified water level data.

Chapter 2 provides specific information about the comparison strategy.

1.3 Outline

The thesis is consist of five chapters. Chapter 1 mainly introduces the background of satellite altimetry technique, the previous studies and history of the development of the densification method, as well as the motivation and outline of this work. Chapter 2 explains detailed information regarding data and survey specifications such as the survey area and the studied river, the selected combination of altimetric satellite missions, the gauging stations and virtual stations along the river. Chapter 3 presents the primary methodologies for the data densification method. The kernel procedures for the densification, such as modelling river flow velocity or modelling covariance functions for observations, are introduced in details. After that, some additional statistical methods are also described to ensure the consistency for comparison, e.g., the non-linear least squares estimation, data snooping, and interpolation method. Chapter 4 demonstrates the results and related analyses for the densification, e.g., specific graphical comparisons with zoomed-in figures, as well as a general numerical comparison in a table. Chapter 5 contains the conclusion part of the work and also an outlook for the future. Besides, a few less important but relevant examines are also included in the appendix as well.

Chapter 2

Data and Survey Specifications

2.1 Combination of Satellite Missions

To ensure the consistency of comparison for two densification methods, the combination of the altimetric satellite missions should remain the same. In this work, water level time series at virtual stations are recorded by six different satellites. All data from those missions are applied to the two methods. This section introduces the information about combined satellite missions as well as their temporal and spatial resolutions and durations.

2.1.1 TOPEX/Poseidon and TOPEX Extended Mission²

TOPEX/Poseidon was an ocean TOPOgraphy EXperiment mission launched in 1992 by the National Aeronautics and Space Administration (NASA) and the Space Agency of France (CNES). It reached an accuracy of 4.2 cm for the measurement of sea surface topography. It allowed for an improved study of ocean circulation and a better understanding of global warming phenomenon. Thanks to TOPEX, researchers successfully predicted the *El Niño* phenomenon between 1997 and 1998. Although initially it was planned to carry out the main task for three years and equipped with consumable storage for five years, TOPEX has surprisingly provided 13 years data with an unprecedented precision of better than 5 cm. The TOPEX extended mission was a follow-on mission of TOPEX and started in September 2002. Finally, the mission ended in January 2006.

2.1.2 ENVISAT and ENVISAT Extended Mission³

ENVISAT (ENVironmental SATellite) was a satellite mission launched by the European Space Agency (ESA) in May 2002. It was supposed to be the largest civilian Earth observation mission. It was equipped with ten measurement instruments and weighed

²<https://sealevel.jpl.nasa.gov/missions/topex>.

³<https://earth.esa.int/web/guest/missions/esa-operational-eo-missions/envisat>.

up to eight tons. It carried advanced radar altimeter, imaging radar, temperature radiometer to monitor various information about the Earth within, its atmosphere, land, water, ice and environment. Regarding a wide range of applications for many scientific activities and researches, the ENVISAT mission was decided to be extended voted by the ESA Member States. However, the extended mission ended in April 2012 with an unexpected loss of contact.

2.1.3 OSTM/JASON-2⁴

OSTM/JASON-2 (Ocean Surface Topography Mission) was a mission operated by the NASA and the CNES to monitor the sea surface topography. It was launched in June 2008 and it was the follow-on mission to TOPEX and JASON-1. Its designed duration was three years. However, its running time was actually ten years. Thanks to its onboard Poseidon-3 dual-frequency altimeter, advanced microwave radiometer, and DORIS instruments, JASON-2 allowed to monitor global sea level changes from space observing systems.

2.1.4 SARAL/ALTIKA⁵

SARAL (Satellites with ARGos and ALTika) was a complementary mission to JASON-2. The mission was supposed to run for five years for Argos (Advanced Research and Global Observation Satellite) and three years for Altika altimeter. It was a joint cooperation between the CNES and the Indian Space Research Organization (ISRO). This mission used the concept of the altimetry to study ocean circulations and sea surface elevation. It significantly improved our knowledge on the sea surface height reconstruction as well as meteorology and sea state forecasting. The SARAL mission was successfully realized in February 2013. In this thesis, we have applied the data from SARAL in 2013 and 2014.

2.1.5 Resolution and Duration for Satellite Missions

In this section, the definitions of the temporal and spatial resolution for satellite altimetry are explained. The temporal resolution depends on the number of passes over the water bodies under study. When multiple missions are not taken into account, the temporal resolution of single satellite altimetry is determined by its repeat period. As for spatial resolution, it is represented by the distance of satellite ground track patterns at the Earth's equator. From Table 2.1, we can see that TOPEX, TOPEX extended mission and JASON-2 are of the same temporal and spatial resolutions. For the other three missions, resolutions are the same, too.

⁴<https://sealevel.jpl.nasa.gov/missions/ostmjason2/>.

⁵<https://earth.esa.int/web/eoportal/satellite-missions/s/saral>.

Satellite Mission	Temporal Resolution [day]	Spatial Resolution [km]	Duration [year]
TOPEX	10	311	1992–2002
TOPEX extended	10	311	2002–2005
JASON 2	10	311	2008–2015
ENVISAT	35	80	2002–2010
ENVISAT extended	35	80	2010–2012
SARAL	35	80	2013–2014

Table 2.1: Combination of different satellite data sets.

2.2 Survey Area and River

This thesis aims to compare the two densification methods under fair circumstance so that the same survey area and studied river should be selected. An Italian river – Po river is chosen and applied for the two methods. Figure 2.1 shows the location and topography of the Po river from the river source to the mouth as well as its basin.



Figure 2.1: Po river from river source to mouth⁶.

The Po river is the longest river in the Northern Italy. It crosses three countries, namely, Italy, Switzerland and France. It flows eastward. In our study, the tributaries of the Po river are not taken into consideration. We have only defined the virtual stations along the main Po river. There are five gauging stations for validation and 43 virtual stations with respect to six different satellite missions along this river. During our work, it turned out that Po river does not possess obvious annual behaviour. This means that the seasonality of Po river is hard to recognize and extract. However, we must remove the seasonal behaviour for the kriging densification method. In order to solve such

⁶<http://www.reizen-langs-rivieren.nl/index.html>.

a problem, we use the annually averaged water levels in 12 months to represent the seasonality. Chapter 3 explained this procedure in detail. Specific information about the Po river are provided in Table 2.2.

Name	Po river
Country	Italy
Source	Monte Viso, elevation of 3700 m, 44°42'N, 7°5'S
Mouth	Adriatic Sea, elevation of 0 m, 44°57'N, 12°25'S
Length	652 km
Basin	70,091 km ²

Table 2.2: Information about Po river⁷.

The terrain of the Po river basin is high in the west and reduces eastwards. The upper west reaches are consist of rolling hills with altitudes over 1,700 m. The middle and lower reaches are the famous Great Plains of the Po river. This area concentrates most of the big lakes in Italy. Although the Po river basin is abundant in water resources, it is not much developed in the middle and lower reaches. Only some water conservancy projects have been built in the upper reaches of some tributaries.

2.3 Gauging Stations

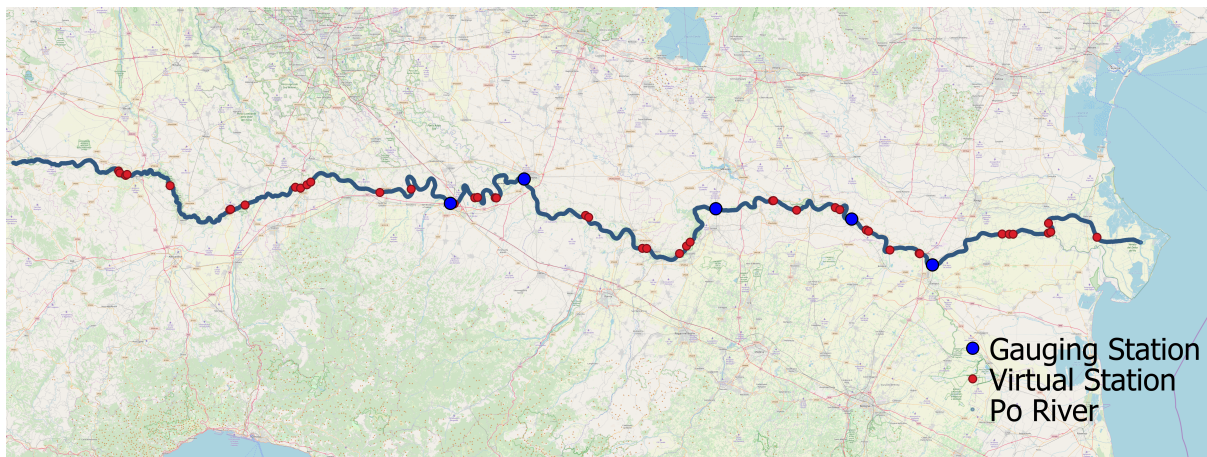


Figure 2.2: Distribution of gauging stations and virtual stations along the Po river.

To ensure the consistency of the comparison, the same gauging stations must be applied for validation between the densified time series of water level and the actual

⁷<https://www.britannica.com/place/Po-River>.

values. As shown in Figure 2.2, there are five gauging stations along the Po river eastwards, namely, Piacenza, Cremona, Borgoforte, Sermide and Pontelagoscuro. The five gauging stations are distributed from the river source to the river mouth along the Po river. Their latitudes and longitudes as well as the corresponding mean water levels are displayed in Table 2.3. In situ water level data are daily collected at five gauging stations.

Gauging Station	Latitude [°]	Longitude [°]	Mean Water Level [m]
Piacenza	45.06	9.70	42.38
Cremona	45.13	10.00	29.04
Borgoforte	45.05	10.75	14.06
Sermide	45.02	11.29	9.50
Pontelagoscuro	44.89	11.61	3.49

Table 2.3: Latitude, longitude, and mean water level at gauging stations along the Po river.

2.4 Virtual Stations

In addition, water level time series at virtual stations along the Po river must be the same for the two densification methods. Figure 2.3 demonstrates the temporal synoptic visualization of water level time series at all virtual stations along the Po river over 26 years.

According to this picture, there are generally six altimetric missions and 43 measurements along the Po river. Each satellite mission only collects data within a specific time period, from half a year to ten years. Time series of water level at the single virtual station is not meaningful for hydrological studies for the whole river. That is a reason why the combination of altimetric observations at various virtual stations to produce a densified time series is significant. Chapter 3 introduces these two densification methods. Besides, Tables 2.4 and 2.5 provide specific information about the defined virtual stations along the Po river.

Note that differently from the hydraulic statistic densification by Tourian et al. (2016), altimetric data from the CryoSat-2 mission are not included in the densification production in our work. Because, we need to keep consistent for the set of applied satellite combinations. In order to realize the kriging densification method by Boergens et al. (2017), we need to transform the original time series of water level into the residual time series. However, we could not acquire residual time series for CryoSat-2, since the repeat period of CryoSat-2 is too long, i.e., 369 days. Obtaining a time series with such long repeat period is impossible. Therefore, the CryoSat-2 mission is excluded in our work for both densification methods.

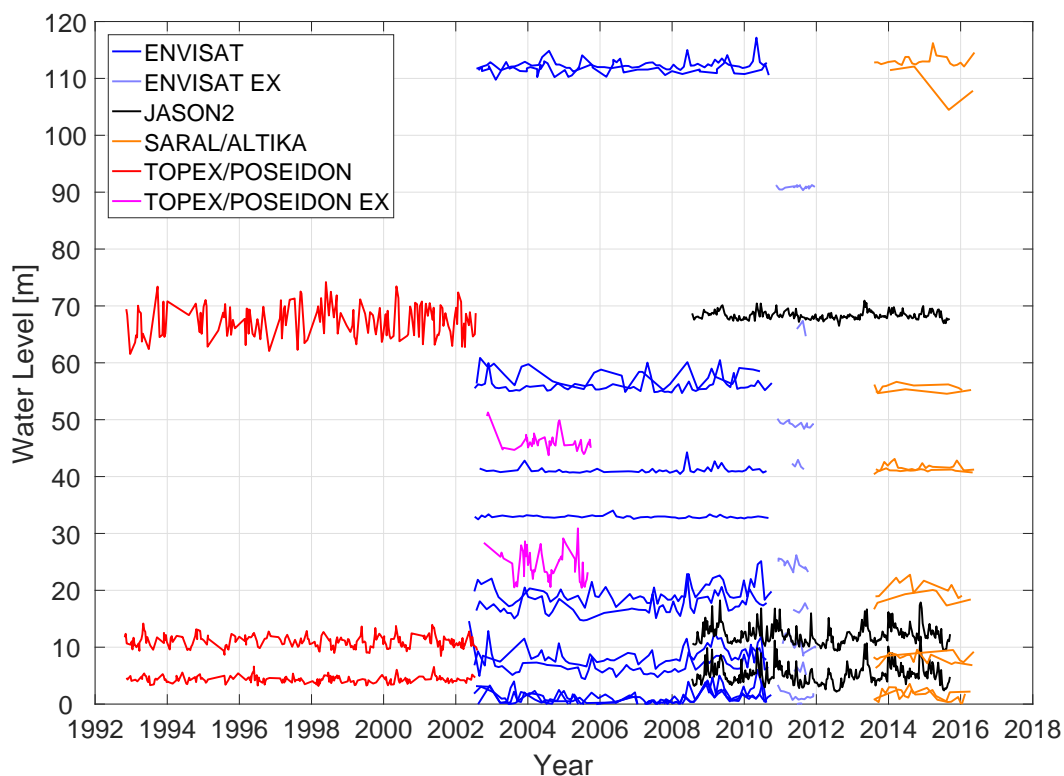


Figure 2.3: Synoptic visualization of water level time series at all virtual stations between 1992 and 2018.

Additionally, to inspect the influence of CryoSat-2, we have made a test in the densification process. Two attempts – one with CryoSat-2, the other one not, have been carried out with the hydraulic statistic densification method. Results and more details can be found in Appendix A. It can be seen that using or excluding CryoSat-2 altimetric data has no significant effects for the hydraulic statistic densification. This results indicates that removing CryoSat-2 has not much influence for our comparison between the two densification methods.

Count Nr.	Mission	Track	Mean Level [m]	Latitude [°]	Longitude [°]	River Width [m]
1	ENVISAT	108	112.43	45.15	8.39	280
2	SARAL	216	113.07	45.15	8.40	270
3	SARAL	801	108.96	45.14	8.42	270
4	ENVISAT	401	111.74	45.14	8.42	130
5	ENVISAT ex	734	90.90	45.11	8.59	230
6	JASON2	9	68.34	45.04	8.83	290
7	TOPEX	9	67.31	45.04	8.83	290
8	ENVISAT ex	689	66.15	45.06	8.89	520
9	ENVISAT	337	55.94	45.11	9.09	290
10	SARAL	674	55.69	45.10	9.11	330
11	SARAL	257	55.19	45.11	9.14	350
12	ENVISAT	129	57.83	45.12	9.15	330
13	ENVISAT ex	188	49.24	45.09	9.42	400
14	TOPEX ex	120	46.11	45.10	9.55	520
15	ENVISAT ex	143	42.00	45.06	9.71	350
16	ENVISAT	65	41.13	45.08	9.80	250
17	SARAL	130	41.67	45.08	9.81	230
18	SARAL	715	41.10	45.08	9.88	480
19	ENVISAT	358	32.94	45.08	9.89	540
20	ENVISAT ex	504	24.51	45.03	10.24	350

Table 2.4: List for defined virtual stations along the Po river.

Count Nr.	Mission	Track	Mean Level [m]	Latitude [°]	Longitude [°]	River Width [m]
21	TOPEX ex	85	24.35	45.02	10.25	230
22	ENVISAT	294	19.60	44.94	10.46	230
23	SARAL	588	20.36	44.94	10.48	270
24	ENVISAT ex	459	16.76	44.92	10.61	240
25	SARAL	171	18.50	44.94	10.64	320
26	ENVISAT	86	17.30	44.95	10.65	300
27	JASON2	120	12.16	45.07	10.98	330
28	TOPEX	120	11.03	45.07	10.98	330
29	ENVISAT ex	820	10.73	45.04	11.07	230
30	ENVISAT	22	8.67	45.05	11.23	420
31	SARAL	44	8.32	45.04	11.24	550
32	SARAL	629	7.91	44.99	11.35	350
33	ENVISAT	315	6.82	44.98	11.36	390
34	ENVISAT ex	775	6.06	44.93	11.44	280
35	JASON2	85	5.21	44.92	11.56	400
36	TOPEX	85	4.35	44.92	11.56	400
37	ENVISAT ex	274	1.58	44.98	11.89	500
38	ENVISAT	251	1.51	44.98	11.91	450
39	SARAL	502	1.57	44.98	11.93	500
40	SARAL	85	1.75	44.98	12.07	340
41	ENVISAT	43-01	0.92	44.98	12.08	360
42	ENVISAT	43-02	1.10	45.00	12.07	440
43	ENVISAT ex	229	-0.05	44.97	12.26	650

Table 2.5: List for defined virtual stations along the Po river (Continuation of Table 2.4).

Chapter 3

Methodology

In order to overcome the limitations of low temporal and spatial resolutions of water level time series by single altimetric mission, the densification methods by combining all available altimetry missions along a river have been developed. There are two proven densification methods so far. The first method is a hydraulic statistic densification method published by Tourian et al. (2016). It is based on the flow velocity of rivers and time lags between virtual stations. The second approach is a kriging densification method developed by Boergens et al. (2017). It is based on the kriging interpolation and covariance function. Thanks to these densification methods, it is possible to obtain a densified time series with higher resolutions both in space and time. Besides, there are some other processing steps applied to both densification methods, e.g., non-linear least squares estimation. This chapter provides the specifics about the methodologies for the entire implementation procedure of the two densification methods.

3.1 Hydraulic Statistic Densification Method

We refer to the first method as the hydraulic statistic densification process due to the combination of hydraulic and statistical procedures for the densification. It is based on the river flow velocity and the resulting time lag shifts between virtual stations. Thanks to these added temporal shifts on the original time series, a merging of altimetric water level data is possible.

3.1.1 Overview of Densification Procedure

To implement the hydraulic statistic densification method, we have taken the following steps:

- (i) Estimate river flow velocity model calculated by the river width and river slope.
- (ii) Estimate time lag between virtual stations and add the lag time to the densified time series.

- (iii) Normalize observed time series, which is needed because different time series of water level are not at a same elevation. This can be seen in Figure 2.3.
- (iv) Apply a data snooping to remove outliers in the normalized time series.
- (v) Rescale normalized time series to the corresponding water level heights to construct new densified time series.

Details about velocity model estimation and rescaling are explained below. The data snooping algorithm, which is applied to both densification methods, are described in section 3.4 in details.

3.1.2 Estimation of Parameters and River Velocity Model

In order to be consistent with Tourian et al. (2016), we have calculated the parameters and river velocity model for the hydraulic statistic densification at the beginning. The biases between different satellites can be derived from cross-calibration in line with Bosch et al. (2014). They are defined as deviation of differences between altimetric time series and averaged time series at gauging stations. In that study, they compared altimetric data from three tide gauging stations, i.e., Rovinj, Venezia, Trieste over the Adriatic Sea. It turned out in their study that all satellite missions measured the water level with small biases.

As for the velocity model along the Po river, needed data can be provided and estimated at the gauging stations, such as river discharge. River flow velocity can be estimated as discharge divided by river sectional area. Moreover, river width can be estimated by the imaginary processing of LANDSAT. River slope is defined below:

$$S = \frac{\Delta H_g}{\Delta L_g} = \frac{H_i - H_{i-1}}{L_i - L_{i-1}}. \quad (3.1)$$

Herein, ΔH_g is the elevation difference between gauging stations. ΔL_g is the horizontal distance between gauging stations. Note that ΔL is not directly linear distance, but the absolute distance along the Po river which can be obtained using coordinates along the river. According to Fig. 3.1, some periodic trends of the measurements are displayed at gauging stations.

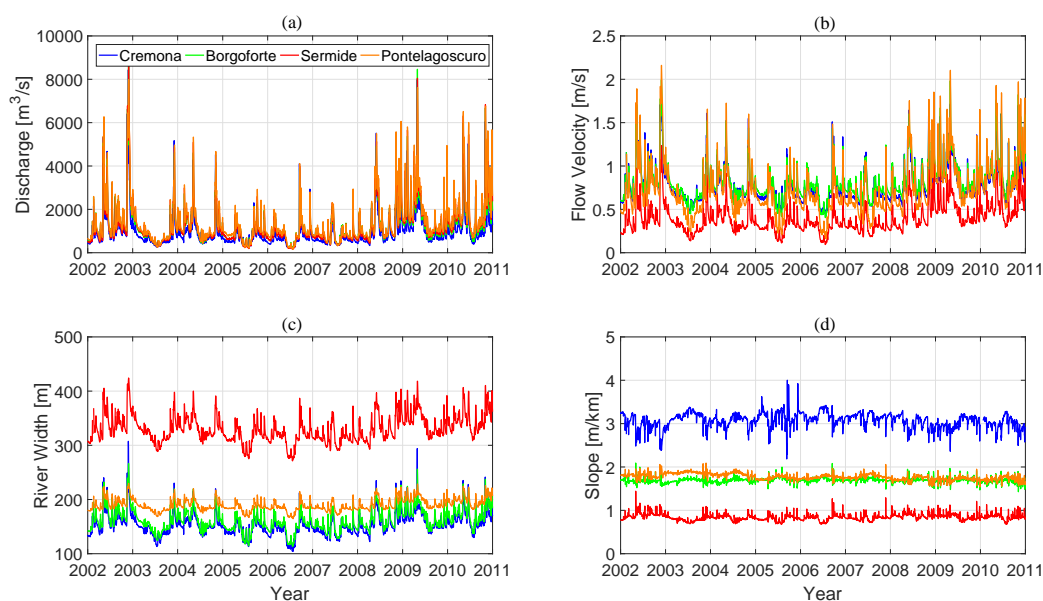


Figure 3.1: Variations of (a) river discharge, (b) river flow velocity, (c) river width, and (d) river slope at four gauging stations Cremona, Borgoforte, Sermeide and Pontelagoscuo between 2002 and 2011.

Due to the motivation of hydraulic statistic densification, we wish to connect the time series of water level at various virtual stations. Thanks to the two discharge models developed by Bjerklie et al. (2005), it is possible to make a transformation to obtain a river flow velocity model only based on river width and river slope. Two discharge models are shown below:

$$\mathbf{Q} = k_1 \mathbf{W}^p \mathbf{V}^q \mathbf{S}^t, \quad (3.2)$$

and

$$\mathbf{Q} = k_2 \mathbf{W}^s \mathbf{V}^t, \quad (3.3)$$

where, \mathbf{Q} is discharge, \mathbf{W} is river width, \mathbf{S} is river slope, and k , p , q , r and s are model parameters to be estimated.

Note that time series of water level at each gauging station is used for calculation of the parameters at the next gauging station. The reason is that for river slope, differences between the elevations and horizontal distances are both needed. With two sets of observations, we can only obtain one set of differences. Time series at the first gauging station was only used as a reference, i.e., its slope cannot be calculated.

The next step is to generate these two aforementioned discharge models by using non-linear least squares technique. The idea is to minimize the norm of model error of Dennis Jr and Schnabel (1996) and calculate the model parameters k , p , q , r and s . To that end, we apply the averaged discharge $\bar{\mathbf{Q}}$, averaged river width $\bar{\mathbf{W}}$, averaged river

slope \bar{S} , and averaged river velocity \bar{V} from the in situ data. Eventually, we obtain the following discharge models:

$$\bar{Q}_1 = 0.23\bar{W}^{1.00}\bar{V}^{2.50}\bar{S}^{-0.49}, \quad (3.4)$$

$$\bar{Q}_2 = 0.31\bar{W}^{1.65}\bar{V}^{1.67}. \quad (3.5)$$

By combining and rearranging models (3.3) and (3.4), we could acquire a general flow velocity model for the Po river as a function of river width and river slope. This is illustrated in the following.

First of all, we assume that the discharges in different models are constant:

$$\bar{Q}_1 = \bar{Q}_2. \quad (3.6)$$

By replacing of Eqs. (3.4) and (3.5), we arrive at the following equation:

$$0.23\bar{W}^{1.00}\bar{V}^{2.50}\bar{S}^{-0.49} = 0.31\bar{W}^{1.65}\bar{V}^{1.67}. \quad (3.7)$$

Then we classify the parameters and make a rearrangement:

$$\frac{\bar{V}^{2.50}}{\bar{V}^{1.67}} = \frac{0.31}{0.23} \cdot \frac{\bar{W}^{1.65}}{\bar{W}^{1.00}} \cdot \frac{1}{\bar{S}^{-0.49}}. \quad (3.8)$$

At the end, we use the mean values to represent the general velocity model:

$$V = 1.45W^{0.79}S^{0.59}. \quad (3.9)$$

Note that the velocity here needs to be distinguished with the velocity in the models (3.2) and (3.3). Here it is a predicted velocity model over the whole river. The velocity along the Po river can be estimated at any given locations. However, in Eqs. (3.2) and (3.3), V is only the flow velocity collected at the gauging stations. It is not universal, but nevertheless can be applied to validate the predicted velocity model (3.9).

Finally, we obtain the river flow velocity model with averaged gauging data to represent the whole river. In order to validate it and assess its stability, we compare the predicted model (3.9) against the actual velocity data at gauging stations. As shown in Fig. 3.2, we make a calculation to evaluate the quality of predicted velocity model.

The residual flow velocity is defined as below:

$$V_{\text{residual}} = |V_{\text{predicted}} - V_{\text{real}}|. \quad (3.10)$$

The root-mean-squared errors (RMSE) of the velocity model can be calculated as:

$$\text{RMSE} = \sqrt{\frac{\sum_1^n (V_{\text{predicted}} - V_{\text{real}})^2}{n}}. \quad (3.11)$$

The relative root-mean-squared errors (rRMSE) of the velocity model can be estimated. These rRMSE are relative errors in percentages in contrast to the RMSE. It could be calculated as:

$$\text{rRMSE} = \frac{\text{RMSE}}{\bar{V}_{\text{real}}} \times 100\%. \quad (3.12)$$

Herein, \bar{V}_{real} is the mean value of observed velocity. The relative root-mean-squared error is also referred to as normalized root-mean-squared error. The rRMSE of flow velocity at four gauging stations are calculated, respectively around 20%, 20%, 26%, and 35%. These results suggest that the predicted velocity model of Eq. (3.9) has an averaged rRMSE about 25%. Such uncertainties are consistent with the bias errors. In statistics, the RMSE reflects the dispersion of data. Because the actual experimental results could contain positive and negative deviations relative to the averaged value, and the RMSE could eliminate such symbolic effects. Moreover, the rRMSE indicate somewhat the accuracies of data in percentage.

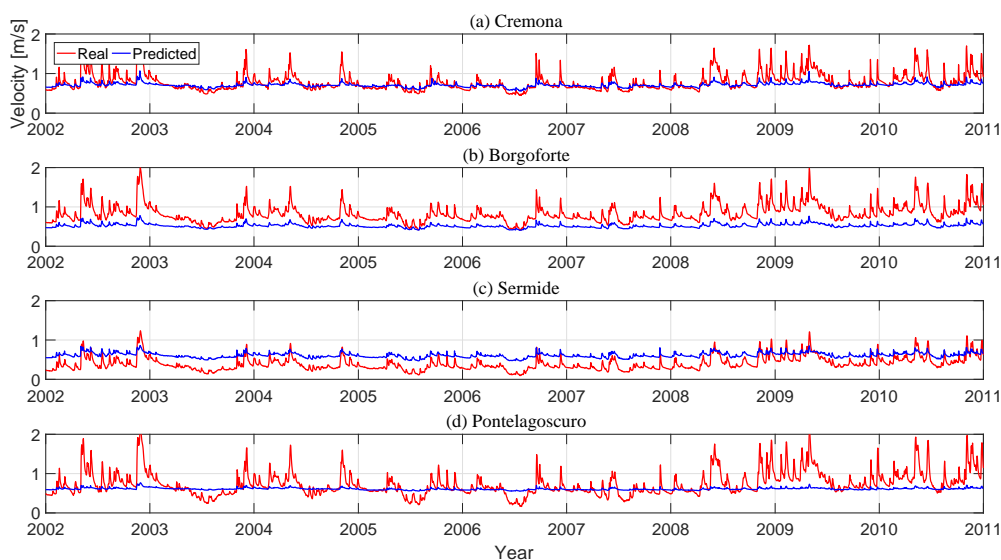


Figure 3.2: Relative root-mean-squared errors of flow velocity models at four gauging stations Cremona, Borgoforte, Sermide and Pontelagoscuro. Errors are: (a) 20.55%, (b) 20.37%, (c) 26.39%, (d) 35.33%. RMS of real flow velocity are: (a) 6.79, (b) 7.00, (c) 4.96, (d) 6.75. RMS of residual data are: (a) 3.21, (b) 4.49, (c) 3.74, (d) 4.21. The red lines reveal the real velocities at the gauging stations. The blue lines reveal the predicted velocities.

Eventually, we can see that errors of the velocity model are increasing along the river course from river source to mouth. The predicted velocities at Sermide and Pontelagoscuro are not as satisfactory as those at Cremona and Borgoforte. The possible reason is that the slopes at the latter two gauging stations are smaller. Those predicted velocities, especially at Pontelagoscuro, are almost constant with rare variations. Therefore, the corresponding rRMSE values are increasing.

3.1.3 Estimation of Time Lag between Virtual Stations

Once we acquire the prediction of flow velocity over the river, it is possible to estimate the time lags between virtual stations. In line with Tarpanelli et al. (2013), the time lag T_L is represented as below:

$$T_L = \frac{L_v}{c}, \quad (3.13)$$

where L_v is the distance between virtual stations and c is the celerity. Similarly, L_v is not the directly linear distance between virtual stations but the absolute distance along the river.

In accordance with Ponce (1989), the celerity is defined as:

$$c = b \cdot V, \quad (3.14)$$

where b is constant and $b = \frac{5}{3}$.

Thus, Eq. (3.13) can be rearranged as:

$$T_L = \frac{L_v}{c} = \frac{L_v}{bV} = \frac{3}{5} \cdot \frac{L_v}{V}. \quad (3.15)$$

We can estimate the time lags thanks to the distances between virtual stations and our predicted velocity model. Afterwards, we obtain connections between all the virtual stations along the Po river with each other. Connections are hereafter referred to as the time lags. The time series are linked with each other in the time domain. The results are displayed in Fig. 3.3. It takes around four days for the water to flow through the first virtual station to the last one. Availability of river slopes, allows to define a reference location at any given coordinate for the purpose of merging all the water level time series. The water level hydrograph at each virtual station has been shifted respectively according to those time lags.

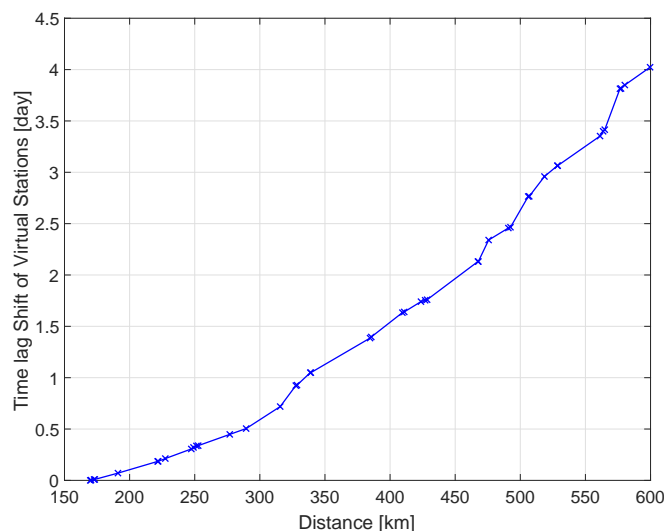


Figure 3.3: Time lags of virtual stations along the Po river. Crosses here are referred to as the defined 43 virtual stations along the river.

3.1.4 Combination of Altimetric Time Series and Reconstruction

The combination procedure of time series of water level and their transformation into corresponding water level heights are the symbols of a successful merging (Tourian et al., 2016). To achieve this, we use algorithms developed by Birkinshaw et al. (2010). The first step is to normalize all the observed water level between zero and one because they are not in a standard height interval. Then it is necessary to apply a Student t -test of 99% to create a limit for the confidence region. After that, outliers can be identified and discarded. In doing so, all data outside the confidence region are seen as outliers. Eventually, the processed time series of water level will be rescaled to the corresponding level heights and the new time series will be constructed.

The reconstruction or rescaling is a reverse process of normalization. For both of normalization and rescaling, we apply a simple linear model. For example, if we make sure that values of original time series are within $[(TS_{old})_{min}, (TS_{old})_{max}]$, where $(TS_{old})_{min}, (TS_{old})_{max}$ are respectively the minimum and maximum values in the original time series. And the values of predicted time series are within $[(TS_{new})_{min}, (TS_{new})_{max}]$, where $(TS_{new})_{min}, (TS_{new})_{max}$ are respectively the minimum and maximum values in the predicted time series. It is easy to simulate the relationship between the original and predicted data by a linear model, as follows:

$$TS_{new} = K \cdot TS_{old} + b. \quad (3.16)$$

Herein, K and b are the parameters for the linear model,

$$K = \frac{(TS_{new})_{max} - (TS_{new})_{min}}{(TS_{old})_{max} - (TS_{old})_{min}},$$

$$b = \frac{(TS_{old})_{max} \cdot (TS_{new})_{min} - (TS_{new})_{max} \cdot (TS_{old})_{min}}{(TS_{old})_{max} - (TS_{old})_{min}}.$$

Using these parameters, we can easily transform the original time series into a new one within different height interval. Besides, the normalization of water level time series at each virtual station is acquired by assigning the 3% and 85% values of the height interval, from minimum to maximum, respectively to zero and one. These choices of 3% and 85% are determined by experiments and finally by the judgements of the best results. This procedure is significant to identify outliers and to evaluate the standards of measurements at virtual stations along the river. In order to identify the outliers, an iterative data snooping method by Baarda (1968) has been applied. This approach may face a risk of losing data to a certain degree. However, it has own advantages, i.e., to combine the weighted standard deviation (see Section 3.4) and outlier removing procedure together. Thanks to this combination, it does not just search for large value but compares data with own standard deviation to identify the extreme values. Such strategies could help to a larger extent to remove outliers correctly so that rescaling and reconstruction of a merging time series remain stable and correct.

3.2 Kriging Densification Method

The kriging method was initially developed for geostatistical spatial data by Krige (1952). It was an interpolation method based on a known covariance of observed and predicted positions. In recent years, it has been widely used not only in space field but also in time field with different observations. To apply the kriging method, we need to know the statistical correlation among the observations. Moreover, the dependencies of spatio-temporal structures are estimated by using covariance functions. There are quite a few models to describe these dependencies (De Cesare et al., 2001) by choosing different objectives and will be explained in this section.

3.2.1 Introduction of Ordinary Kriging

Kriging interpolation is a spatial interpolation method in geostatistics. Here, the word interpolation refers to prediction as well. According to Boergens et al. (2017), kriging is an optimal unbiased estimator to solve the mean-squared interpolation error. If we derive the spatial kriging into two-dimensions, we can obtain the spatio-temporal kriging.

Generally, the prediction in kriging at a unique location in space and time $p(s_0, t_0)$, referred to as the predictor, can be calculated with a weighted mean:

$$p(s_0, t_0) = \sum_{i=1}^n \lambda_i Z(s_i, t_i), \quad (3.17)$$

Herein, $Z(s_i, t_i)$ are entire observations and λ_i are weights of observations. The weights λ_i could be calculated through the dependencies of measurements covariance. For all observations, the weight array can be represented as:

$$\boldsymbol{\lambda} = [\lambda_1, \lambda_2, \dots, \lambda_i]^T. \quad (3.18)$$

We expect the predicted value to be truth so that we could obtain:

$$E\{p(s_0, t_0)\} = E\{Z(s_0, t_0)\}, \quad (3.19)$$

where, E represents the expectation in statistics, which could also be seen as the moment. The moment is a specific quantitative index of a function's shape in statistics (Soliman and Hsue, 1992). If the function represents the distribution of probability, the total probability, i.e., one, is the zeroth moment. The mean is the first moment. This concept is very close to the moment in physics.

In order to apply the kriging method, the stationarity is a vital factor and should be explained as well. In mathematics, the stationary process is a special stochastic process in which the joint probability distribution in a period or space is equal to the joint probability distribution of the new period after arbitrarily shifting. Therefore, mathematical expectations and variances do not change with time or position variations:

$$\begin{aligned} E\{Z_t\} &= E\{Z_{t+\tau_t}\}, \\ E\{Z_s\} &= E\{Z_{s+\tau_s}\}, \end{aligned} \quad (3.20)$$

where τ is the spatial and temporal shifting for the observations.

In kriging, a common sub-method referred to as "ordinary kriging" has been applied. In this ordinary kriging, all observations are supposed to be related and applied to build this model:

$$Z(s, t) = \mu + \delta(s, t), \quad (3.21)$$

where μ is the deterministic part of the model and $\delta(s, t)$ is its stochastic part. In our work, as for altimetric time series of water level, μ is supposed to be an unknown constant mean water level. It is supposed to be constant for all observations.

According to (Boergens et al., 2017), the kriging method is commonly applied assuming the stationarity of observations. In other words, data moment in statistics does not depend on relative positions. It is considered that the kriging plays an irrespective

role as long as the data is stationary and the covariance model reflects non-stationarity. This stationarity simplifies the estimation of the covariance function.

3.2.2 Overview of Densification Procedure

In order to implement the kriging densification method, the following steps should be taken:

- (i) Transform all observations into residual time series of water level. This means removing their mean and the seasonal behaviour.
- (ii) Estimate empirical spatial and temporal covariance model. In our work, the spatio-temporal product model of De Cesare et al. (2001) is applied.
- (iii) Fit the empirical covariance models with non-linear least squares estimation.
- (iv) Estimate the weights based upon the residual time series and the fitted model to calculate the densified time series.
- (v) Restore the residual data and add back the previously removed mean and seasonal behaviour of water level.
- (vi) Normalize restored time series into a common interval and apply the data snooping to remove outliers.
- (vii) Rescale normalized data to their corresponding water level heights and construct new densified time series.

3.2.3 Estimation of Residual Time Series of River Water Level

Suggested by Boergens et al. (2017), the kriging densification method only deals with the residual time series of water level. Therefore, a transformation of original altimetric observations is needed. The residual time series are defined as original time series without mean value or seasonal variations. These residuals are regarded as stationary data in our work.

Note that the selected river, Po river, does not contain a very distinct seasonal behaviour compared to some other rivers, such as the Mekong river (Boergens et al., 2017). The original observations in Fig. 3.4 also indicate to this feature. However, not every river has such a typical seasonal behaviour like Mekong river. In order to simulate the seasonality of Po river, we have defined the annually averaged water level heights in 12 months as the seasonality. To achieve this, we have classified and assigned the original observations to 12 different months within a year. The water levels in the same month are gathered and then the extreme values among them are extracted and removed. Here, we have used the Pauta criterion (Zhang and Yuan, 1997). All data beyond a simple 3-times data standard deviations are identified as outliers. Then, the

mean value of remaining data is calculated and regarded as the standard water level height for the corresponding month. Finally, mean water levels of 12 months are calculated and joint together as the seasonal behaviour of the Po river.

Figure 3.4 displays an example for the transformation process from JASON-2 mission (track number nine). Accordingly, the annual behaviour is logically reflected. The water levels are higher in summer and lower in autumn, and then increase somewhat in winter. It indicates that the precipitation quantity of Po river increases in summer. By removing the mean value and seasonal behaviour, finally we obtain the residual time series represented by the red line.

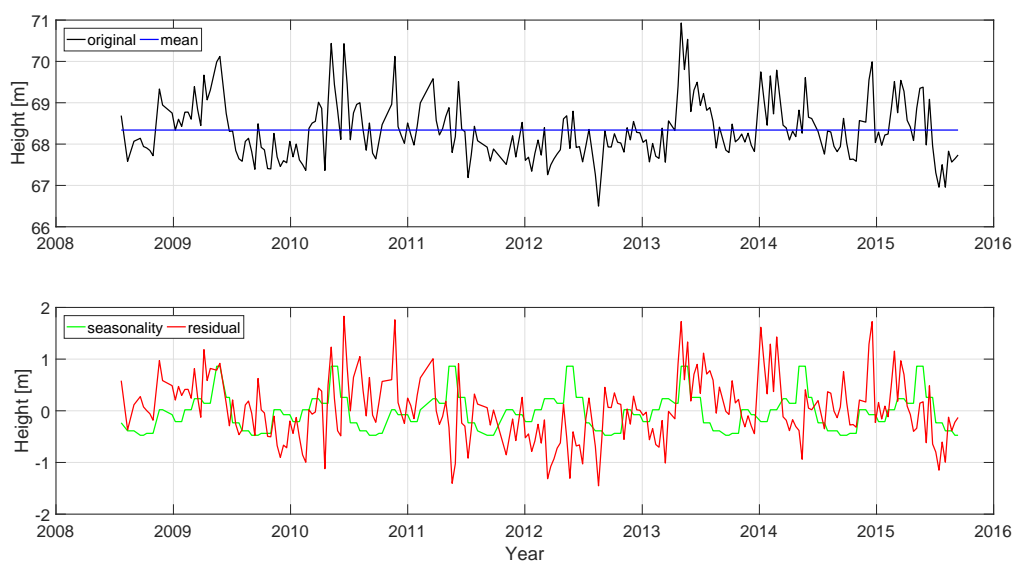


Figure 3.4: Example of observation transformation to residual time series (Jason-2). The black line represents the original time series of water level. The blue line is the mean value. The green line reveals the seasonal variations of the Po river. The red line is the residual time series.

Note that we have also removed the trend represented by a moving average to calculate the residual time series at the beginning. However, after personal communications with Eva Boergens, we decided not to remove the trend to be consistent with Boergens et al. (2017).

3.2.4 Estimation of Spatio-temporal Covariance Model

A suitable spatio-temporal covariance model is a precondition of kriging densification method. Thanks to the covariance model, all altimetric time series of water level could be connected with each other. The relationships of stream variations along the river are revealed by the covariance model.

To estimate such a model, first of all, an empirical covariance matrix should be calculated. Following the ideal of De Cesare et al. (2001), the spatio-temporal correlation can be formed in various ways. Among them, a general model consist of products and sums of spatio-temporal covariance is represented as below:

$$C_{st}(\tau_s, \tau_t) = k_1 C_s(\tau_s) C_t(\tau_t) + k_2 C_s(\tau_s) + k_3 C_t(\tau_t), \quad (3.22)$$

where C_s and C_t are respectively spatial and temporal covariance models. And, k_1, k_2 , and k_3 are coefficients with $k_1 > 0, k_2, k_3 \geq 0$. τ_s and τ_t are respectively spatial and temporal lags for the data.

If we assume that $\tau_s = |s_1 - s_2|, \tau_t = |t_1 - t_2|$, Eq. (3.22) can be derived as:

$$C_{st}((s_1, t_1), ((s_2, t_2))) = k_1 C_s(|s_1 - s_2|) C_t(|t_1 - t_2|) + k_2 C_s(|s_1 - s_2|) + k_3 C_t(|t_1 - t_2|), \quad (3.23)$$

From the general model of Eq. (3.22), it is possible to derive a simple covariance model for stationarity. If we set $k_1 = 1$, and $k_2, k_3 = 0$:

$$C_{st}(\tau_s, \tau_t) = C_s(\tau_s) C_t(\tau_t). \quad (3.24)$$

By applying the same assumption, we can obtain:

$$C_{st}((s_1, t_1), ((s_2, t_2))) = C_s(|s_1 - s_2|) C_t(|t_1 - t_2|). \quad (3.25)$$

This product model is one of the simplest models for spatio-temporal correlations. In particular, it assumes that the spatial and temporal parts do not interacted. On the one hand, the temporal dependence structure is supposed to be invariant in space. On the other hand, the spatial dependence is supposed not to vary with time. This characteristic of separation allows us to respectively fit a spatial covariance model and a temporal covariance model in our work.

Based upon Cressie (1992), if a random field is stationary, where

$$C(x_i, x_j) = C(x_i + \tau, x_j + \tau), \quad (3.26)$$

for any lag τ , the covariance function can be derived with one parameter:

$$C(\tau) = C(0, \tau) = C(x, x + \tau), \quad (3.27)$$

which is called covariogram or covariance function. It is positive definite. Besides, it can be used to estimate of $C(x_i, x_j)$:

$$C(x_i, x_j) = C((x_j + \tau) - (x_i + \tau)) = C(x_j - x_i). \quad (3.28)$$

Under the assumption of the product model of Eq. (3.24), a covariance function can be found in a relevant study by Boergens et al. (2017):

$$C_{st}(\tau_s, \tau_t) = \frac{1}{|N(\tau_s, \tau_t)|} \sum_{(s_1, t_1, s_2, t_2) \in N} Z(s_1, t_1) Z(s_2, t_2), \quad (3.29)$$

where $|N(\tau_s, \tau_t)|$ is the cardinality and $Z(s_i, t_i)$ refers to as the assemblage of all observations. In this work, $Z(s_i, t_i)$ is the residual altimetric time series as mentioned before. It assumes that residual data are a realization of the mean-zero random process and reveal the deviation from the mean seasonal river level in space and time (s_i, t_i) .

However, there is no detailed explanation about implementation of the model of Eq. (3.29) in the paper of Boergens et al. (2017). We have followed the idea of kriging about dealing with the spatial data. Because the temporal data and the spatial data can be handled separately, then model above can be further derived as:

$$C_s(\tau_s) = \frac{1}{|N(\tau_s)|} \sum_{(s_i, s_j) \in N} Z(s_i) Z(s_j), \quad (3.30)$$

and

$$C_t(\tau_t) = \frac{1}{|N(\tau_t)|} \sum_{(t_i, t_j) \in N} Z(t_i) Z(t_j), \quad (3.31)$$

equivalently,

$$C(\tau_m) = \frac{1}{|N(\tau_m)|} \sum_{(m_i, m_j) \in N} Z(m_i) Z(m_j), \quad (3.32)$$

where, τ_m is either the spatial lag or the temporal lag between the i -th and j -th measurements m_i and m_j .

Here, we want to obtain a general model of Eq. (3.32) for both spatial and temporal covariance functions. In order to explain more specifically, Table 3.1 shows a random example as below:

Symbol	m	s	t	Z
Parameter	Order	Space	Time	Residual time series
Unit	[-]	[km]	[day]	[m]
Data	1	4	1	0.8
	2	7	2	0.6
	3	15	3	1.4
	⋮	⋮	⋮	⋮

Table 3.1: Random example of parameters of covariance functions. m is the order of observations. s is the distance from the river source. t is the data observing time. Z is the residual time series of water level.

We can obtain:

$$\begin{aligned} |t_i - t_j| &= \tau_t, \\ |s_i - s_j| &= \tau_s, \\ |m_i - m_j| &= \tau_m. \end{aligned} \quad (3.33)$$

Herein, i and j are the count number of measurements. We set $i < j$.

By replacement, Eq. (3.32) can be derived as:

$$C(\tau_m) = \frac{1}{|N(\tau_m)|} \sum_{(m_i \in N)} Z(m_i)Z(m_i + \tau_m). \quad (3.34)$$

Furthermore, we transform Eq. (3.34) into a general formula to calculate both spatial and temporal covariance functions. To achieve this, we assume that the order of observations m_i equals to natural number i (i.e., $i = 1, 2, 3, \dots$), and $Z(m_i) = Z(i) = Z_i$. Eq. (3.34) can be derived as:

$$\hat{C}(\tau_m) = n^{-1} \sum_{i=1}^{n-\tau_m} Z_i Z_{i+\tau_m}, \quad (3.35)$$

where $n = |N|^{-1}$. i equals the count number for the residual observations. τ_m is the lags between the count numbers and refer to as integer between zero and $n - 1$:

- (i) If $\tau_m = 0$, $\hat{C}(0) = n^{-1} \sum_1^n Z_i^2$,
- (ii) If $\tau_m = 1$, $\hat{C}(1) = n^{-1} \sum_1^{n-1} Z_i Z_{i+1}$,
- ⋮
- (iii) If $\tau_m = n - 1$, $\hat{C}(n - 1) = n^{-1} \sum_1^1 Z_i Z_{i+n-1} = n^{-1} Z_1 Z_n$.

If we set $Z_i = X_i - \bar{X}$, where \bar{X} is the sample mean, we get:

$$\hat{C}(\tau_m) = n^{-1} \sum_{i=1}^{n-\tau_m} (X_i - \bar{X})(X_{i+\tau_m} - \bar{X}), \quad (3.36)$$

where, \bar{X} represent the mean value of the data set.

The covariance matrix of the observations can be derived as:

$$\begin{aligned}
COV &= [\hat{C}(\tau_m)] \\
&= \begin{bmatrix} \hat{C}(0) & \hat{C}(1) & \hat{C}(2) & \dots & \hat{C}(n-1) \\ \hat{C}(1) & \hat{C}(0) & \hat{C}(1) & \dots & \hat{C}(n-2) \\ \hat{C}(2) & \hat{C}(1) & \hat{C}(0) & \dots & \hat{C}(n-3) \\ \dots & \dots & \dots & \dots & \dots \\ \hat{C}(n-1) & \hat{C}(n-2) & \hat{C}(n-3) & \dots & \hat{C}(0) \end{bmatrix}, \\
&= \begin{bmatrix} \sum_1^n Z_i^2 & \sum_1^{n-1} Z_i Z_{i+1} & \sum_1^{n-2} Z_i Z_{i+2} & \dots & \sum_1^1 Z_i Z_{i+n-1} \\ \sum_1^{n-1} Z_i Z_{i+1} & \sum_1^n Z_i^2 & \sum_1^{n-1} Z_i Z_{i+1} & \dots & \sum_1^2 Z_i Z_{i+n-2} \\ \sum_1^{n-2} Z_i Z_{i+2} & \sum_1^{n-1} Z_i Z_{i+1} & \sum_1^n Z_i^2 & \dots & \sum_1^3 Z_i Z_{i+n-3} \\ \dots & \dots & \dots & \dots & \dots \\ \sum_1^1 Z_i Z_{i+n-1} & \sum_1^2 Z_i Z_{i+n-2} & \sum_1^3 Z_i Z_{i+n-3} & \dots & \sum_1^n Z_i^2 \end{bmatrix} \cdot n^{-1}, \\
&= \begin{bmatrix} 0 & 0 & \dots & 0 & Z_1 & Z_2 & \dots & Z_n \\ 0 & \dots & 0 & Z_1 & Z_2 & \dots & Z_n & 0 \\ \dots & \dots & \dots & \dots & \dots & \dots & \dots & \dots \\ 0 & Z_1 & Z_2 & \dots & Z_n & 0 & \dots & 0 \end{bmatrix} \cdot \begin{bmatrix} 0 & 0 & \dots & 0 \\ 0 & \dots & \dots & Z_1 \\ \dots & 0 & \dots & Z_2 \\ 0 & Z_1 & \dots & \dots \\ Z_1 & Z_2 & \dots & Z_n \\ Z_2 & \dots & \dots & 0 \\ \dots & Z_n & \dots & \dots \\ Z_n & 0 & \dots & 0 \end{bmatrix} \cdot n^{-1}. \quad (3.37)
\end{aligned}$$

Note that as shown in Table 3.1, the time lag τ_t could consist the lag of the count number τ_m in certain cases, e.g., for continued daily temporal series without interruption, $\tau_m = \tau_t$. The calculation for covariance model of Eq. (3.31) could be simplified:

$$\hat{C}(\tau) = n^{-1} \sum_{i=1}^{n-\tau} Z_i Z_{i+\tau}. \quad (3.38)$$

This covariance matrix of Eq. (3.37) is a non-negative defined. Besides, it is symmetric and its diagonal elements represent the relationships of the residual data with each other. This indicates that elements near the diagonal parts should be larger as the elements in surrounding areas.

Next procedure is to fit the empirical covariance function by using non-linear least squares estimation. The spatial and temporal covariance function could be estimated separately as previously mentioned. Based on Cressie and Huang (1999), the spatial covariance function is fitted by a linear tent model:

$$C_s(\tau_s) = \begin{cases} a_1 + n_1 & \tau_s = 0 \\ \max\{a_1 - b_1 \cdot \tau_s\} & \tau_s \neq 0, \end{cases} \quad (3.39)$$

where $a_1 > 0$, $b_1 > 0$, $n_1 \geq 0$.

Similarly, according to Boergens et al. (2017), the temporal covariance function is fitted by an exponential model:

$$C_t(\tau_t) = \begin{cases} a_2 + n_2 & \tau_t = 0 \\ a_2^{-b_2 \cdot \tau_t} & \tau_t \neq 0, \end{cases} \quad (3.40)$$

where $a_2 > 0$, $b_2 > 0$, $n_2 \geq 0$.

To simplify the calculation process, the correlation functions instead of related covariance model are fitted. By assuming that $a_1 + n_1 = 1$, $a_2 + n_2 = 1$, there are only four parameters left to be calculated. Figure 3.5 displays the obtained fittings.

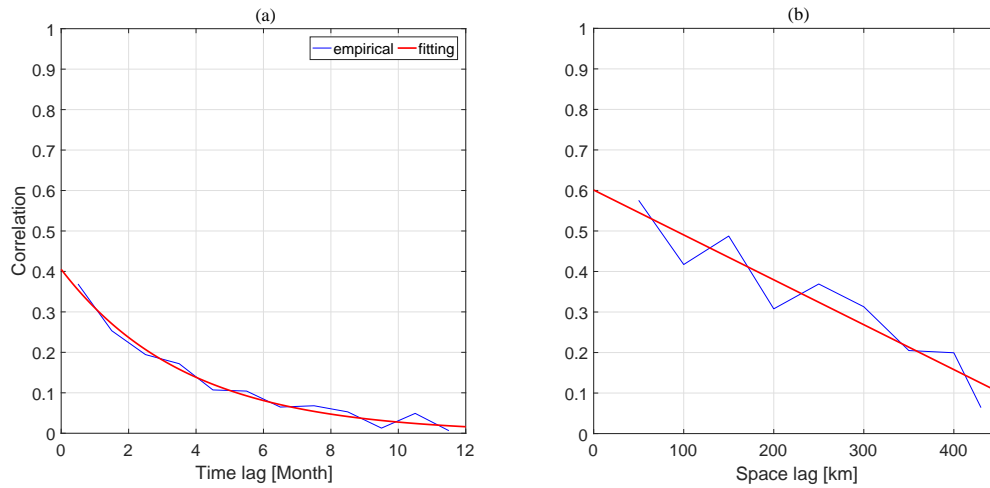


Figure 3.5: Empirical covariance models and the corresponding fittings in time and space.

By applying non-linear least squares estimation, we estimate the parameters in the empirical fitting models. The results are provided in Table 3.2. There are apparent decays in both models. From such a behaviour, we draw a logical conclusion: When the spatial or temporal lags are smaller, the corresponding data play a more significant role.

Spatial Linear Tent Model	a_1	b_1
	0.6010	0.0011
Temporal Exponential Model	a_2	b_2
	0.4052	0.2685

Table 3.2: Parameters of the fitting model.

Having the fitting models estimated, we can now easily calculate the spatial and temporal covariants using Eqs. (3.35), (3.37) and (3.38) for a giving point with known space and time locations (s_0, t_0) .

3.2.5 Estimation of Weights and Consequent Predicted Water Level Time Series

Thanks to kriging interpolation method, connections between the residual observations and the predictor $p(s_0, t_0)$ can be derived:

$$p(s_0, t_0) = \sum_{i=1}^n \lambda_i Z(s_i, t_i), \quad (3.41)$$

where, λ is the weight and $Z(s_i, t_i) = \{(s_1, t_1), \dots, (s_n, t_n)\}$ represents the residual time series. For verification, we make the following test:

$$\sum_{i=1}^n \lambda_i = 1. \quad (3.42)$$

Eq. (3.42) indicates that the weights of all residuals should add up to one for the unbiased prediction.

The weights could be estimated using the following formula:

$$\lambda_{n \times 1} = \left[\left(\mathbf{c} + \mathbf{l} \frac{(1 - \mathbf{l}^T \mathbf{C}_{st}^{-1} \mathbf{c})}{\mathbf{l}^T \mathbf{C}_{st}^{-1} \mathbf{l}} \right)^T \right] [\mathbf{C}_{st} + \mathbf{C}_{alti}]^{-1}, \quad (3.43)$$

where $\mathbf{l}_{n \times 1} = [1, \dots, 1]^T$ is a unit array. $\mathbf{c}_{n \times 1} = [c((s_0, t_0), (s_1, t_1)), \dots, c((s_0, t_0), (s_n, t_n))]^T$ is the predicted correlations between the observed residuals and densified time series. $\mathbf{C}_{st} = [C((s_i, t_i), (s_j, t_j))]_{i,j=1, \dots, n}$ represents the covariance matrix. \mathbf{C}_{alti} is a diagonal matrix of relative accuracies between the observations of altimetric missions. The matrix dimensions of \mathbf{C}_{st} and \mathbf{C}_{alti} are the same. Additionally, with the help of personal communications, the ENVISAT mission is chosen to be the reference because of the large number of available long time series with acceptable accuracies. Table 3.3 displays these information per mission. Since the weights for all observations are estimated, it is possible to compute the predicted residual time series at any known locations or at any given time.

Mission	ENVISAT/ ENVISAT EX	SARAL	JASON-2	TOPEX/ TOPEX EX
Accuracy [cm]	4.5	3.4	3.3	4.2

Table 3.3: Accuracies of satellite missions⁸.

3.2.6 Restore and Combination

From the predicted residual data to the final densified time series, we still need a few more procedures. First of all, the predicted time series should be restored. This means that the previously removed mean values and seasonal components should be added back. To ensure the coherence, we have classified the residuals due to their virtual station names. This allows us to add the mean values and the seasonal components back in sequence given by virtual stations. The next procedure is a normalization of the restored data within $[0, 1]$, since the restored data are not in a common height interval. Then we have applied data snooping to remove outliers with respect to the standard deviations. Finally, the normalized data are rescaled back to their corresponding water level heights and the new densified time series is created. This final step guarantees the consistency between the two densification methods.

3.3 Non-linear Least Squares Estimation

Among the densification process, the non-linear least squares estimation plays a significant role to estimate the unknown coefficients in models and ensuring a consistent comparison between the two methods. Traditionally, there are two kinds of algorithms: The searching algorithm and the iterative algorithm. In this work, in order to solve the non-linear least squares problem, we apply the iterative algorithms. This procedure is explained below:

- (i) Estimate non-linear observation equations $y = f(x)$. y and x are the output and input of system. f is a function between y and x .
- (ii) Estimate approximate initial values x_0 .
- (iii) Realize the linearisation, $\Delta y(x_0) = A(x_0)\Delta x + e$. Δy and Δx are the small increments in output and input. A is the design matrix. e is the error.
- (iv) Estimate unknown parameters, $\Delta \hat{x} = [A^T(x_0)A(x_0)]^{-1} A^T(x_0)\Delta y(x_0)$.
- (v) Update approximate values, $\hat{x} = x_0 + \Delta \hat{x}$.
- (vi) Calculate iteratively until the stop criteria is fulfilled, i.e., $||\Delta \hat{x}|| < \epsilon = 10^{-6}$.

⁸Available from <https://www.nasa.gov/> and <https://m.esa.int/ESA>.

The most critical step here is the linearisation. Generally the observation equations are not linear, which means that a linearisation is needed. There are many ways to realize the linearisation and we choose a conventional one: Expansion of a Taylor series:

$$\sum_{n=0}^{\infty} \frac{f^{(n)}(a)}{n!} (x-a)^n = f(a) + \frac{f'(a)}{1!} (x-a) + \frac{f''(a)}{2!} (x-a)^2 + \dots \quad (3.44)$$

In our work, the non-linear least squares algorithm is applied to estimate the parameters not only in the river velocity model by the hydraulic statistic densification, but also in the empirical covariance function by the kriging densification.

3.4 Data Snooping Method

To remove outliers in the densified time series, specific statistical methods are used. At the beginning, we tested the Pauta criterion (Zhang and Yuan, 1997). It identifies outliers beyond a simple 3-times data standard deviation (STD). However, the outcome of this test turned out to be unsatisfactory. Subsequently, we applied a data snooping. In a common data snooping method, the largest values are identified as outliers by an iterative process. Differently, in our work, larger values with respect to their own standard deviations are identified as outliers iteratively. These outliers are removed and excluded from the final densified time series.

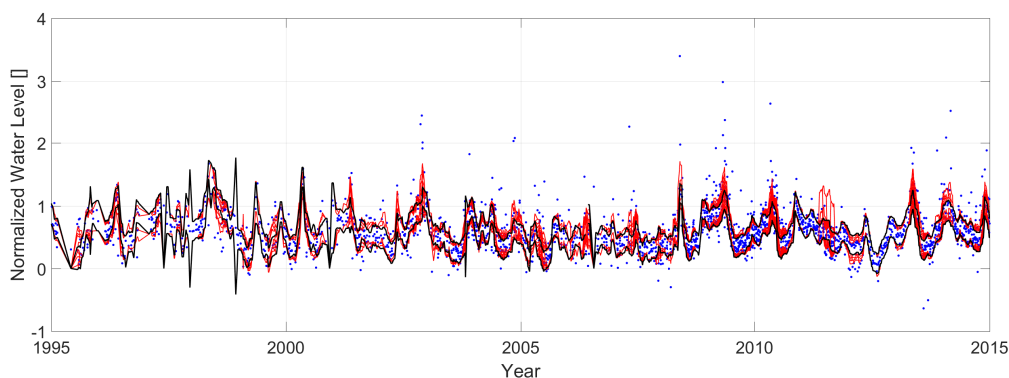


Figure 3.6: Example of data snooping at the gauging station Piacenza between 1995 and 2005. The blue points are the densified time series of water level. The two red lines are the upper and lower limitations of the confidence intervals for every iteration. The two black lines are the final interval limitations.

The weighted standard deviation can be estimated as follows:

$$\delta = \sqrt{\frac{\sum w_i (y_i - \bar{y}^*)^2}{\frac{n-1}{n} \sum w_i}}. \quad (3.45)$$

Herein, y_i is an observation. w_i is the corresponding weight. \bar{y}^* is the weighted mean. n is the total number of all observations. The weight and the weighted mean can be calculated as follows:

$$\bar{y}^* = \frac{\sum w_i y_i}{\sum w_i}, \quad (3.46)$$

$$w_i = \frac{1}{\text{STD}^2}. \quad (3.47)$$

Having the weighted standard deviation obtained, we can realize further needed processing steps in our data snooping. The steps are listed below:

- (i) Define a sliding time window with 30 days. It scans the total observation time series. Such window length is recommended by Tourian et al. (2016). On the one hand, the longer sliding window could not identify the outliers very well. On the other hand, the shorter window length may take the risk of losing data.
- (ii) Apply a Student's t-test with a 99% confidence limit to identify the inconsistent measurements, namely, outliers.
- (iii) Estimate the upper and lower limits:

$$l_{up/low} = \mu \pm \left[t_0 \cdot \frac{\delta}{\sqrt{n-1}} + d \right]. \quad (3.48)$$

Herein, μ is the mean value. t_0 is distributed as t-test. $n - 1$ is the free degree of the sampling data. δ is the weighted standard deviation as Eq. (3.45). d is a flexible adjustment to protect the water level highs and lows. Suggested by Tourian et al. (2016), $d = 0.15$.

- (iv) Scan the entire time series with time shifting iteratively. In each turn, the biggest outlier compared to the weighted standard deviation is removed until no data out of the confidence limits are found.

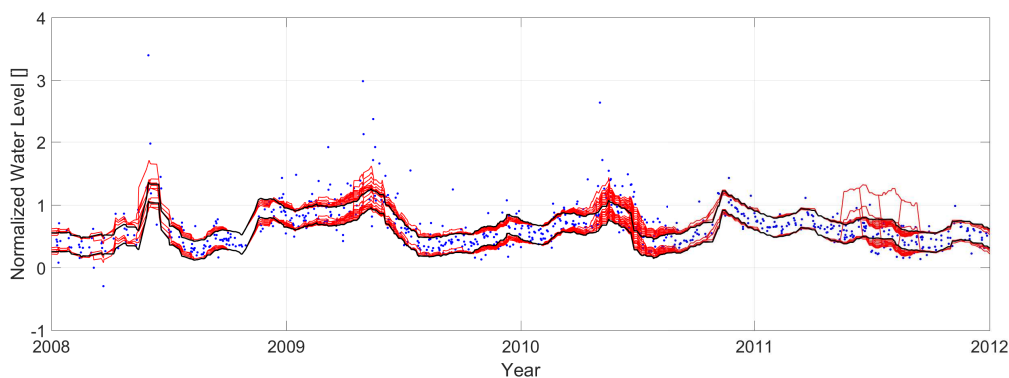


Figure 3.7: Zoomed-in figure for details display between 2008 and 2012. The blue points are the densified time series of water level. The two red lines are the upper and lower limitations of the confidence intervals for every iteration. The two black lines are the final interval limitations.

Figures 3.6 and 3.7 visualized data snooping procedure applied for densified time series at the gauging station Piacenza. It is clear that the upper and lower boundaries of the confidence interval are greatly overlapped with each other. The reason is that as long as a point is identified as outlier and removed, limitations of confidence interval are recalculated. Hence, the upper and lower limitations are varying in time during this iterative process. Only the points between these two black lines are regarded as valid data and are kept for further works. As shown in pictures, there are many points referred to as outliers using the applied data snooping.

3.5 Interpolation Method

In our work, the densified time series by the hydraulic statistic method achieve a temporal resolution of three days. As for the kriging densification method, we can implement the predictions at any given time so that its temporal resolution can be defined whatever needed. In order to compare the two methods under the same circumstances, we have defined the resolution for the kriging method as a three-day one, too.

After the densified time series of water level is generated, we need to compare the results with in situ data statistically. However, the defined three-day temporal resolution of the densified time series is lower than the sampling rate for gauging stations, namely daily. In order to estimate the statistics of differences such as root-mean-squared errors, and evaluate the densified data, it is necessary to either under sample the in situ data

or interpolate the densified time series. These under sampling and interpolation steps are described below:

- (i) The first alternative is a down-sampling of in situ data. We can extract single point out of every three water heights. This way, we can reduce the resolution of the in situ data to three days, i.e., the same as densified time series of water level.
- (ii) Alternatively, it is also possible to apply the interpolation method to the densified time series. We can interpolate points within known data. It allows us to improve the resolution of the densified time series to a single day.

We tested the both alternatives. The results demonstrate negligible differences in statistical comparison. Eventually, we decided to leave in situ data intact. The interpolation was applied to densified time series to allow for a comparison between the in situ data and the densified time series.

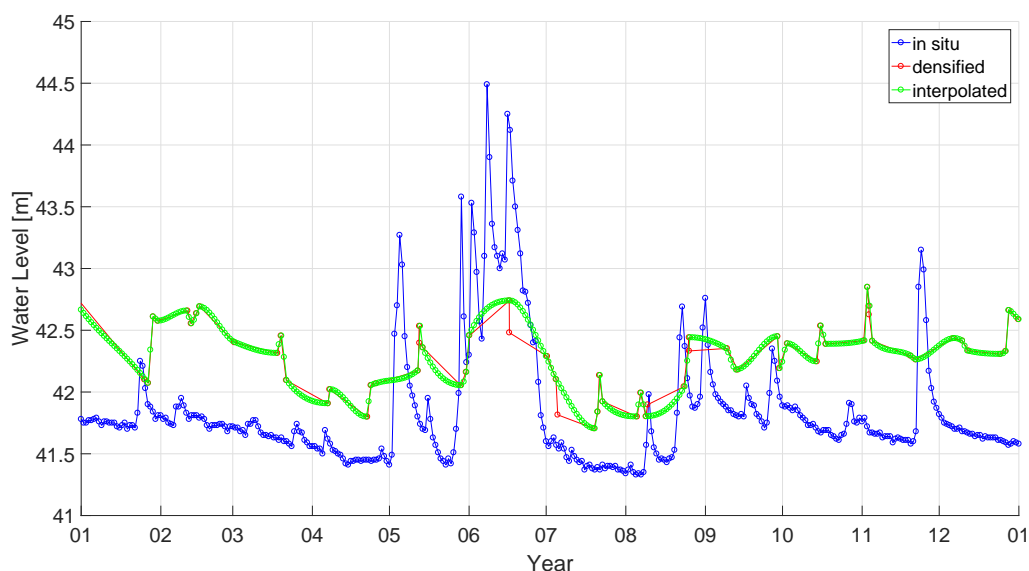


Figure 3.8: The zoomed-in densified time series as well as interpolated data against daily in situ at gauging station Piacenza in year 2007. The red line is the original densified water level time series. The blue line is the in situ data at gauging station. The green one is the interpolated densified time series with cubic interpolation.

Figure 3.8 allows for a visual comparison between the densified time series and its interpolated variant against the daily in situ data in the year 2007. Generally, there are a few different approaches to implement the interpolation, e.g., linear interpolation, cubic interpolation. Linear interpolation is a method of curve fitting using a linear polynomial, while cubic interpolation gives a special spline polynomial. In our test, it turns out that the cubic interpolation is more robust than the linear interpolation, and it conforms better to the in situ data with smaller errors. Thanks to the interpolation method, we can make a quantitative comparison between the densified time series and the in situ data.

Chapter 4

Comparison and Analysis

4.1 Comparison of Densification Methods

In this section, the two densification methods are compared with each other, and their similarities and differences are discussed.

4.1.1 Similarities

- (i) The same original data are used when implementing the two methods, e.g., the same altimetric time series of water level at virtual stations, and the same in situ data at gauging stations.
- (ii) The corresponding height interval of water level in the same location along the river remains the same for the two densification methods. Along with the river course eastwards, the elevations of the river decline gradually. To simplify the calculation, we divide up the river into sections based on the locations of virtual stations. In each section, the corresponding height interval is estimated. To achieve this, we select reference sections along the river. As shown in Fig. 2.3, the altimetric missions containing long durations or a large number of observations are chosen as references, namely, TOPEX, ENVISAT, and JASON-2. As mentioned in section 3.1, the 3% and 85% values of the height interval, from minimum to maximum, are assumed to be the limitations of height interval at such reference locations. After that, the corresponding height interval in other sections (not the reference) can be derived thanks to the decrement of elevation in proportional to horizontal distance variation from the nearest reference location.
- (iii) The method to normalize various time series to a common interval $[0, 1]$ or rescaling procedure from $[0, 1]$ to corresponding water level heights should be kept the same for both densification methods. A simple linear model is applied with the combination of a Student's t-test (see Section 3.1). Note that the rescaling process has a significant effect. After personal communications with Eva Boergens, we realized that in the work of Boergens et al. (2017), the densified time series are interpolated with certain in situ data when rescaling. Such behaviour makes the

results close to the in situ data and less convincing. Hence, for more conclusive comparison, we decided to exclude in the situ data in rescaling step and apply the same algorithm in hydraulic statistic densification (Tourian et al., 2016) for that purpose. Hence, the in situ time series are only used for validation in our work and do not possess any other influence on the any intermediate steps in the implementation procedure.

- (iv) The approach to remove outliers for densified time series remains constant for both methods. An advanced data snooping mention the t-Student's test is applied with respect to the data's standard deviation.

4.1.2 Differences

- (i) The basis of the hydraulic statistic densification method is to estimate the river flow velocity model along the river. Time lags between virtual stations could be calculated, and adjustments of time shifting are added up to the observed water level time series.
- (ii) The basis of the kriging densification method is to estimate the statistical covariance function and the covariance matrix depends on all observations. Therefore, the densified time series of water level can be predicted as a function of entire observations.

4.2 Validation of Hydraulic Statistic Densification Method

In this section, the results of the hydraulic statistic densification method are validated against gauging data. It is already described that we can obtain the densified time series of water level at any given time and any given location. In order to compare them with the in situ data, we produced densified time series at five gauging stations.

Figure 4.1 reveals that the densified time series of water level have quite similar behaviours as the in situ data. The predicted time series of water level follow the in situ data to a large degree. Such results indicate to a successful implementation of the densification algorithms. We also perform a statistical comparison in Table 4.1.

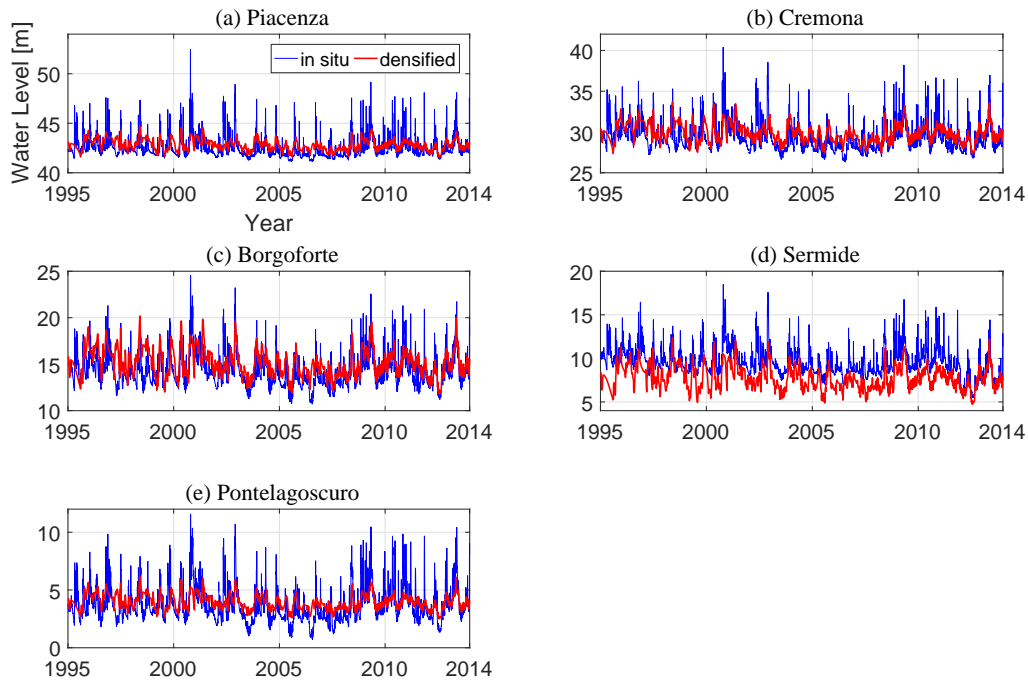


Figure 4.1: Hydraulic statistic method densified water level time series against in situ data at five gauging stations: (a) Piacenza, (b) Cremona, (c) Borgoforte, (d) Sermide, (e) Pontelagoscuro between 1995 and 2014. The red line shows the densified water level time series. The blue line is the in situ data.

In situ data	Piacenza	Cremona	Borgoforte	Sermide	Pontelagoscuro
MAX	52.45	40.40	24.54	18.47	11.56
MIN	41.16	26.34	10.70	5.48	0.74
MEAN	42.34	28.96	13.95	9.16	3.42
STD	1.08	1.70	1.81	1.64	1.56
Densified data					
MAX	44.86	34.05	20.61	12.78	6.35
MIN	41.40	26.96	11.36	4.35	2.33
MEAN	42.78	29.78	15.01	7.68	3.92
STD	0.54	1.10	1.44	1.32	1.63
Residuals					
MAX	7.59	6.35	3.93	5.69	5.21
MIN	0.24	0.62	0.66	1.13	1.59
MEAN	0.44	0.82	1.06	1.48	0.50
STD	0.54	0.60	0.37	0.32	0.93

Table 4.1: Statistics (m) of differences between time series densified based on the hydraulic statistic densification method and in situ data at five gauging stations.

From Table 4.1, we can identify some important features. First thing needs to be noticed is that the predictions at the fourth station (Sermide) is seriously biased compared to those obtained at other stations. It has the largest deviation of mean differences (1.48 m) between the predicted time series and in situ data. The possible reason for that could be the errors in the flow velocity model.

If we look into the river flow velocity in Section 3.1, it is easy to find out that velocities predicted at the latter two stations (Sermide and Pontelagoscuro) are less accurate with larger rRMSE values. Due to the importance of the velocity model in hydraulic statistic densification process, these inaccurate velocities can lead to the height interval deviation.

Secondly, some highs and lows of in situ time series cannot be modelled correctly. Predictions for some water level peaks are neglected and not simulated at all. This loss can be considered as the essential drawback of the densification method. There are various causes for this explanation. On the one hand, extreme values of in situ data may extend beyond the corresponding altimetric water level heights. It means that predicted time series cannot achieve those extremes. The predicted time series only cover the middle part of the in situ data. On the other hand, the extreme highs and lows could mistakenly be identified as outliers in the data snooping. They are mistakenly removed due to iterative processing.

Besides, Table 4.1 shows us that the maximums of the densified time series are smaller than the upper limit of the in situ data. And, the minimums of the densified time series are larger than the lower limit of the in situ data. The reason for that is that the densified time series is more concentrated in the middle elevation due to the data snooping. With it, the off-centred densified data are eliminated. Also, the densified data is more stable than the in situ data with lower standard deviation. Mean values of the densified time series are larger as well. Their standard deviations are smaller than in situ data.

Accordingly, we can assume that the identification of outliers using data snooping could significantly influence the densification process and related results. That is one reason why we apply the same data snooping to both densification methods. This strategy ensures the consistency for the comparison, and the outlier-removing process will not be an influencing factor. This also indicates that the outlier detection scheme may need to be improved further for a future and improved implementation of the densification method.

4.3 Validation of Kriging Densification Method

In this section, the densified time series of the kriging method are validated. Figure 4.2 displays the results of the comparison with the graphic. Table 4.2 provides the corresponding statistics.

Accordingly, somewhat similar features are revealed as the results for the hydraulic statistic densification method. The densified time series of water level have somewhat similar behaviours and follow in situ data to a large degree. This indicates to a successful implementation of the kriging densification method. The densified time series of water level at station Sermide shows a same bias. The same reasons, which are explained in the previous section, could be valid in this case, too.

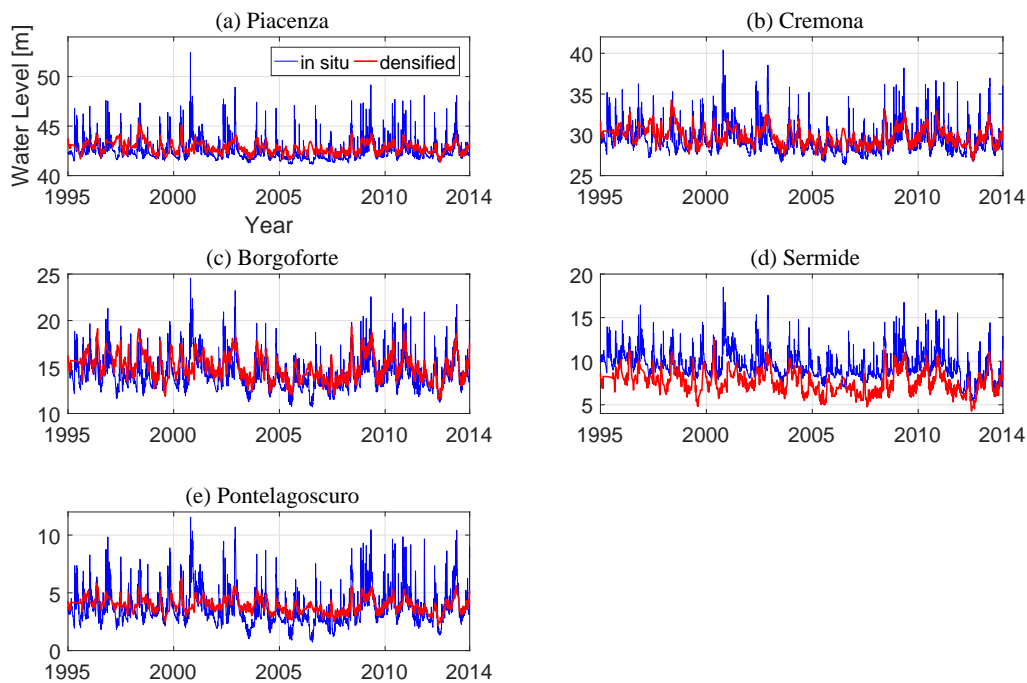


Figure 4.2: Kriging method densified water level time series against in situ data at five gauging stations: (a) Piacenza, (b) Cremona, (c) Borgoforte, (d) Sermide, (e) Pontelagoscuero between 1995 and 2014. The red line shows the densified water level time series. The blue line is the in situ data.

Table 4.2 shows the same features as those for the hydraulic statistic densification method. If we make a comparison between Tables 4.1 and 4.2, it is evident that mean differences of water level, as well as standard deviations for the results by the kriging method, are smaller. This can indicate to more centralized predictions using kriging densification method. Its accuracies also exceed the hydraulic statistic densification method by 2% – 9% improvements.

In situ Data	Piacenza	Cremona	Borgoforte	Sermide	Pontelagoscuro
MAX	52.45	40.40	24.54	18.47	11.56
MIN	41.16	26.34	10.70	5.48	0.74
MEAN	42.34	28.96	13.95	9.16	3.42
STD	1.08	1.70	1.81	1.64	1.56
Densified Data					
MAX	45.31	34.26	20.13	12.57	6.28
MIN	41.35	26.74	11.53	4.27	2.23
MEAN	42.76	29.71	14.96	7.63	3.90
STD	0.57	1.14	1.47	1.35	1.65
Residuals					
MAX	7.14	6.14	4.41	5.90	5.28
MIN	0.19	0.40	0.83	1.21	1.49
MEAN	0.39	0.70	0.94	1.60	0.40
STD	0.51	0.56	0.34	0.29	0.91

Table 4.2: Statistics (m) of differences between time series densified based on the kriging densification method and in situ data at five gauging stations.

4.4 Specific Graphical Comparison

In this section, we proceed with detailed visual comparisons for the two densification methods with three zoomed-in examples extracted at various gauging stations. Each of these cases is chosen because of their individual emphasis and importance. The results can reveal different characteristics of the two densification methods.

4.4.1 Case 1

The first case is selected at the gauging station Cremona between 2010 and 2014. In a common time interval shown in Fig. 4.3 in black boxes, there are many continuing highs of water level within this period, when we look into the in situ data.

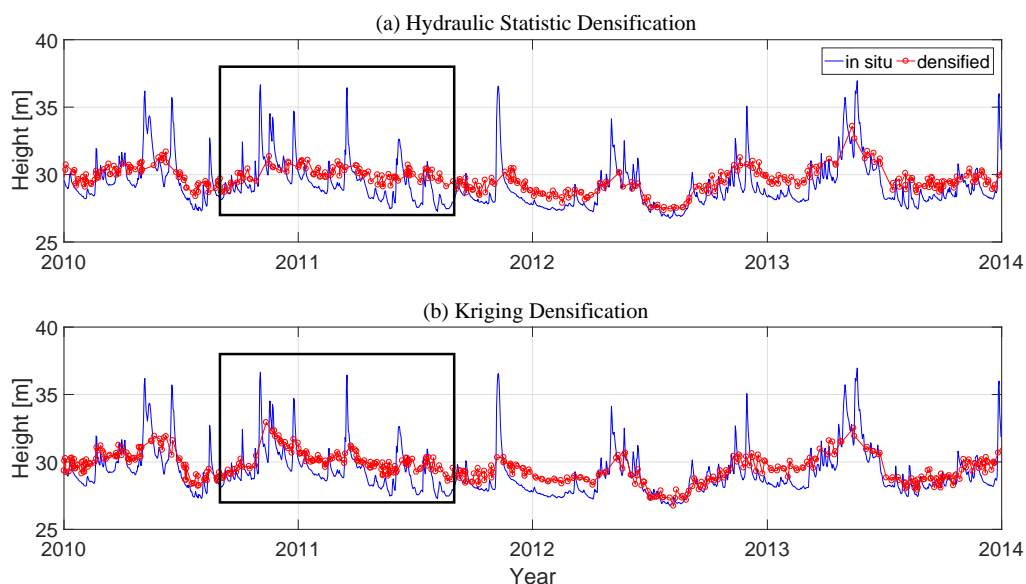


Figure 4.3: First example of detailed comparison at second gauging station Cremona between 2010 and 2014. The red line shows the densified water level time series. The blue line is the in situ data.

The kriging densification method shows a better performance compared to the other method. The time series fragment in Fig. 4.3b associated with the kriging method reflects a better agreement with of water level variations. The highs of water level are distinctly predicted, and they are easier to distinguish. On the contrary, the densified time series related to the hydraulic statistic method in this period contain fewer features. Moreover, the water level highs and lows within the same period in Fig. 4.3a associated with the hydraulic statistic method are lost and cannot be identify.

In this case, the predictions in Fig. 4.3b have a better performance. We can come up with a possible explanation for this behaviour. The kriging densification method mainly focuses on the segments near predictors: Observations with larger spatial or

temporal lags take relatively small weights for predictions calculated in Eq. (3.43). Their impacts on the predictions are negligible. By the kriging method, continuing observations with more water level highs are displayed within this short period and play a more important role when predicting. Those highs affect the predictions by raising the limits for identifying outliers. Consequently, higher water levels in this period remain in the densified time series. On the opposite, the hydraulic statistic densification deals with the total time series, and the reinforcement of such water level highs is avoided.

4.4.2 Case 2

This is a special case selected at the gauging station Borgoforte between 2000 and 2004. Within this common time interval, the two densification methods have different priorities when the level highs are predicted.

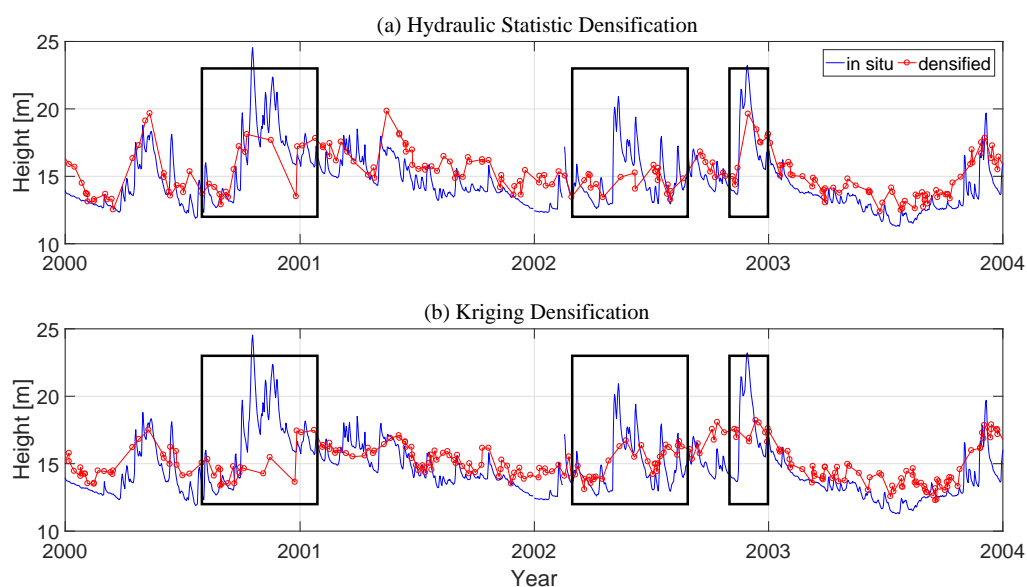


Figure 4.4: Second example of detailed comparison at third gauging station Borgoforte between 2000 and 2004. The red line shows the densified water level time series. The blue line is the in situ data.

Figure 4.4 shows that in the chosen common time interval between 2000 and 2001, shown in with black boxes, the results from hydraulic statistic method are better to predict the highs, while the kriging prediction simply ignores these peaks. However, in the second chosen time interval, the behaviour of methods is completely the opposite. The hydraulic statistic densification ignores those highs, while results associated with the kriging method show a better performance. As for the third chosen time interval, the features are the same as the first one.

According to Fig. 4.4, such interesting results suggest that each of the two densification methods has their own priorities to predict the water level, especially for the catchment of time series peaks. We can see that those peaks within the second chosen common interval are lower than the highs in the other two. Hence, we can assume that the hydraulic statistic densification can show a better performance when predicting extreme water level highs. Thanks to the statistics in Tables 4.1 and 4.2, the kriging method densify the observations into a more centralized height interval, as mentioned in previous section. Thus, the kriging method could have relatively weak control over the extreme values.

4.4.3 Case 3

This particular case is selected at the gauging station Pontelagoscuro. In the selected common time interval, both two densification methods show a poor performance in predicting river level lows.

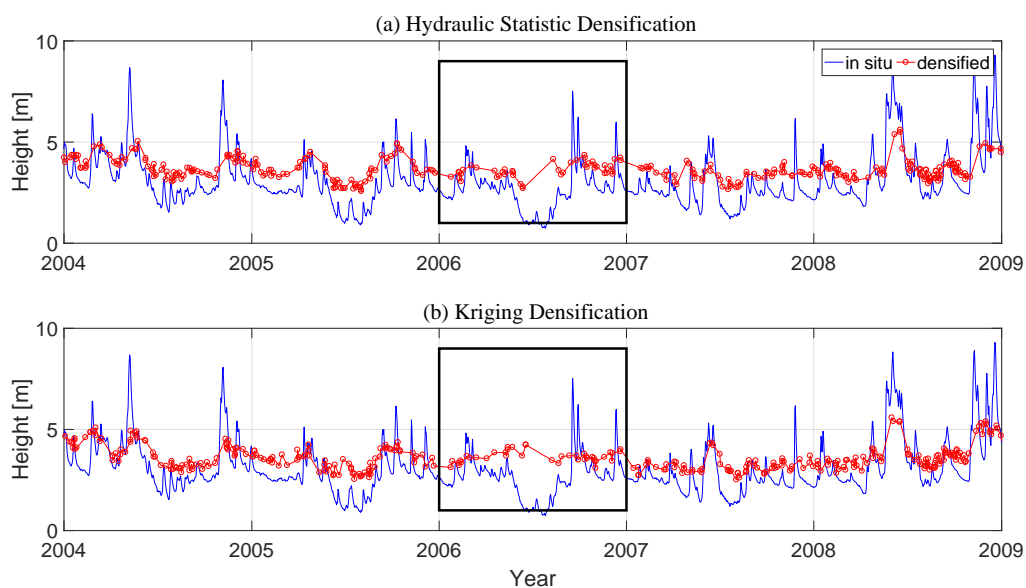


Figure 4.5: Third example of detailed comparison at fifth gauging station Pontelagoscuro between 2004 and 2009. The red line shows the densified water level time series. The blue line is the in situ data.

The in situ data drop down in the selected period. However, neither of the two densification methods captures this feature correctly. Instead, an overall trend is used to cover the whole chosen time interval. The reason can be that most of the low levels within this period are removed as outliers. Only a few measurement remain left for the prediction. Another possible reason could be that the original observations within this period are absent due to technical or man-made causes. These results suggest that in certain cases with extreme values, both densification methods could lead to incorrect simulations.

4.5 General Numerical Comparison of the Densification Methods

In this section, we provide a general numerical comparison between the two densification methods at the five gauging stations. This comparison is indispensable for analysing the results. There are totally five statistics, namely, bias, standard deviation (STD), root-mean-squared error (RMSE), correlation coefficient (CORR) and Nash-Sutcliffe efficiency (NSE) for differences between predicted time series and in situ data. Table 4.3 shows these statistics for both methods. These numbers reveal the quality of predictions as well as the features for the two densification methods.

Gauging Station		Piacenza	Cremona	Borgoforte	Sermide	Pontelago-scuvo
BIAS [m]	HSD	0.44	0.82	1.06	1.48	0.50
	KD	0.39	0.70	0.94	1.60	0.40
STD [m]	HSD	0.54	0.60	0.37	0.32	0.93
	KD	0.51	0.56	0.34	0.29	0.91
RMSE [m]	HSD	0.72	1.07	1.03	0.98	0.81
	KD	0.67	1.01	1.03	1.00	0.87
CORR []	HSD	0.50	0.57	0.65	0.64	0.67
	KD	0.51	0.59	0.64	0.63	0.63
NSE []	HSD	0.31	0.37	0.44	0.44	0.51
	KD	0.32	0.41	0.48	0.46	0.48

Table 4.3: Numerical comparisons between hydraulic statistic densification method and the kriging densification method. Green data suggest a better performance using the kriging densification method. Red data refer to as worse results for the kriging method. Also, HSD = hydraulic statistic densification and KD = kriging densification.

- (i) BIAS here refers to the deviation of the mean water level heights of two different densification methods against in situ data. Note that the corresponding water level heights are the elevation calculated based upon the proportional distance of virtual stations sections (see Section 4.1). Hence, there are indeed deviations between the densified time series and in situ data. The in situ data are only used for final validation in our work.

Except for the gauging station Sermide, BIAS at the other gauging stations is smaller when using the kriging densification method. There are around 11% – 20% improvements. On the opposite, the kriging method is about 8% worse at the gauging station Sermide. Such results indicate that the general deviations when using the kriging densification method are smaller than results using the hydraulic statistic densification method. Hence, the kriging densification method performs better as far as BIAS is concerned.

- (ii) STD values represent the dispersion's degree of a dataset. Sometimes STD values are referred to as accuracies as well. In our work, STD is used to describe the stability and accuracy of the predicted water level time series. From the behaviours of in situ data in Figs. 4.1 and 4.2, it is clear that the time series of water level have its own unique characteristic for data distribution: The majority of water level data varies only in the middle height interval. In contrast, water level peaks arise stochastically with much higher elevations compared to most of the water levels in the time series. Moreover, water level lows stay more steady than the highs.

There is no doubt that the kriging densification method performs better for the STD. In all five gauging stations, the densified time series are improved by using the kriging method by about 2% – 9%. The lower STD can be referred to as more accurate and more concentrated of a dataset. On the opposite, considering the features of water level time series, higher STD means that the highs and lows of water level may take the risk of being dropped out in outlier detection stage, especially for the peaks. In general, one can say that the kriging densification method performs with a better STD than the hydraulic statistic densification method.

- (iii) RMSE is a traditional index to describe the degree of dispersion between observations and values predicted by a model. In our work, RMSE of the densified water level time series for two methods are compared to the standard water levels in situ data. The best results of RMSE should be zero, which means that no deviation exists.

For the RMSE values, differently from the previous two indices, results for two densification methods turn out to be almost the same. Each method separately improves the results at two of the gauging stations by 2% – 7%. The hydraulic statistic method is better at stations Sermide and Pontelagoscuro. The kriging method is better at stations Piacenza and Cremona. Besides, the results remain the same at the third gauging station. Hence, one can state that these two densification methods show approximately similar RMSE numbers against in situ data.

- (iv) The CORR can be estimated as below:

$$\text{CORR} = \frac{\sum(Y_i - \bar{Y}_i)(X_i - \bar{X}_i)}{\sqrt{\sum(Y_i - \bar{Y}_i)^2} \sqrt{\sum(X_i - \bar{X}_i)^2}}, \quad (4.1)$$

where, Y_i is the densified time series, X_i is the in situ time series at the gauging stations, and \bar{X}_i, \bar{Y}_i are the mean values of the corresponding dataset. In statistics, this index is used to measure the difference of two variations. These two variations are mutually independent. CORR is represented by the coefficient within $[0, 1]$. One means that two variations are fully correlated. Zero refers to that they have no connection at all.

For CORR values, the hydraulic statistic densification demonstrates better performance. It provides an approximately 2% – 6% of improvements at Borgoforte,

Sermide and Pontelagoscuo, whereas the kriging densification method performs better (about 3%) at Piacenza and Cremona. Hence, we can draw the conclusion that the hydraulic statistic densification method contains a better performance than the kriging method for index CORR. Though, the improvements are not quite significant.

(v) NSE can be derived as below (McCuen et al., 2006):

$$NSE = 1 - \frac{\sum(Y_i - X_i)^2}{\sum(X_i - \bar{X}_i)^2}, \quad (4.2)$$

where, Y_i is the densified time series, X_i is the in situ time series at the gauging stations, and \bar{X}_i is the mean value of the corresponding dataset. This index is widely used in hydrological applications, and it can provide an indicate on the goodness of a hydrological prediction model. It ranges within $[-\infty, 1]$. One is when the predicted model is excellent with the perfect quality. Zero indicates that the accuracy of the prediction is the same as the mean value of observations. In other words, the predicted model is generally convincing, but the related errors could be large. Moreover, this index can also be negative for an unbiased model, which is supposed to be poorly predicted.

Undoubtedly, the kriging densification method dominates in these NSE values. It is optimal with approximately 3% – 11% improvements except for the last gauging station Pontelagoscuo. Consequently, the predicted time series developed by the kriging densification method possess better NSE index than the hydraulic statistic densification method. We can generally suggest that water level forecasting by using the kriging densification method for the Po river is optimal.

Above analysis involves different statistics (BIAS, STD, RMSE, CORR and NSE) for comparison of the two densification methods. Besides, we can also make a comparison of results between different virtual stations.

Note that for the first three gauging stations Piacenza, Cremona and Borgoforte, the kriging densification method dominates in all five indices. On the opposite, the hydraulic statistic densification method at the latter two gauging stations Sermide and Pontelagoscuo are comparative or even better. Such results are distinctly location relevant, influenced by the distribution of virtual stations. These features could remind us of the aforementioned river velocity model of Eq. (3.9). Compared to the in situ data, the velocities at the last two gauging stations have respectively 6% and 15% more relative errors. This phenomenon is also shown in Fig. 3.2.

Hence, we can make an assumption that the river flow velocity model is connected with the quality of the two densification results. The hydraulic statistic densification method is directly affected by the river flow velocity to calculate the time lags (see Section 3.1). As for the kriging densification method, although the river flow velocity is not directly involved, it is also needed to calculate the corresponding water level heights. In the restore and combination procedures, the normalized data are rescaled

back to their corresponding water level height. In order to make sure that the rescaling process in the two methods is the same, the river flow velocity also plays a role there.

With relatively good predicted velocities at the first three gauging stations Piacenza, Cremona and Borgoforte, the kriging densification method owns a better performance in those five statistics. On the opposite, when the velocities are with great errors, the hydraulic statistic densification method dominates in numerical comparison. However, these speculations still need some more of experiments.

Nowadays, there are many ways to model the river flow velocity with the different combination of parameters. Results always have certain deviations or errors in one way or another compared to the in situ data. Because, the river velocity itself is extremely changeable in time due to various factor, namely, river slope, Earth's topography, the precipitation, and seasonal variations. Such great uncertainties make it almost impossible to acquire for the precise river velocities for every given location. Errors always exist in such velocity models.

Table 4.3 indicates that the hydraulic statistic densification method might perform better than the kriging densification method in those sub-optimal situations and locations, where accuracies of the velocity models are somewhat lower. In such cases, the velocity models along rivers are subject to larger errors. On the opposite, for an excellent velocity model, the kriging densification method is certainly is a better choice according to the conducted numerical comparison.

Chapter 5

Conclusion and Outlook

The time series of water level produced by single altimeter have lower resolution due to the limitation of satellite orbits. Approaches have been developed to combine all available altimetric missions along a river to construct a new densified time series, which is referred to as data densification. To our knowledge, there are only two prove densification methods applied to the river for now. The first is a hydraulic statistic densification method developed by Tourian et al. (2016). The other is the kriging densification method published by Boergens et al. (2017). We implement these two methods and make a visualized comparison. According to these three graphical comparisons in detail, we capture some of the different features and characteristics of the two densification methods. However, we still do not know which one better is. Then we make a general numerical comparison of the results at all five gauging stations. In this chapter, the conclusions of our work based on the previously developed methodologies and results are described. Furthermore, we provide the outlooks for future works to possibly improve the densification methods.

5.1 Conclusion

- (i) Two densification methods are comparable with each other.

The original studies conducted by Tourian et al. (2016) and Boergens et al. (2017) do not allow for a comparison of them. Because, they are realized under different circumstances, e.g., different combinations of satellite missions, two different rivers, different gauging stations, and different virtual stations along the rivers. In our work, we successfully implement these two densification methods under the same conditions. The same river is chosen. The same combination of missions is chosen. And, the same gauging data are used for validation. With such appropriate comparison strategy, these two densification methods can be compared with each other. Densified time series of water level using both densification methods are produced. They reveal somewhat similar behaviours when compared with in situ data. Calculated statistics of these two methods against in situ data are found to be in the same order of magnitude as well.

Note that under applying the hydraulic statistic densification, we typically obtain for the predicted water level time series a temporal resolution of three days. This is a significant improvement compared to the resolution of a single satellite. As for the kriging densification method, we can set the predictors at any given time. To ensure the consistency of the comparison between these two densification methods, we set this three-day temporal resolution for the kriging method, too.

- (ii) Generally speaking, the kriging densification method is found to have a better performance than the hydraulic statistic densification method. Table 5.1 provides information about improvements in percentage using the kriging densification method against the hydraulic statistic densification method.

Gauging Station	Piacenza	Cremona	Borgoforte	Sermide	Pontelagoscuro
BIAS [%]	11	15	11	8	20
STD [%]	5	6	8	10	2
RMSE [%]	7	6	0	2	7
CORR [%]	2	4	2	2	6
NSE [%]	3	11	9	4	6

Table 5.1: Improvements in percentage using the kriging densification method against the hydraulic statistic densification method. Green data suggest a better performance using the kriging densification method. Red data refer to as worse results for the kriging method.

Depending on the statistical results and contrasts in Table 5.1, we can conclude that the densified time series of water level using the kriging densification method outperforms the hydraulic statistic densification method. The improvements are from a few percentages to a maximum of 20%.

However, these improvements are distinctly location relevant. The kriging densification method dominates in all five statistics for the first three gauging stations Piacenza, Cremona, Borgoforte. At the latter two gauging stations Sermide and Pontelagoscuro, the improvements using the kriging densification method are not evident for all statistics. Therefore, follow-up work is still needed in order to obtain more comprehensive, more universal and more reasonable conclusion.

- (iii) The hydraulic statistic densification method has its own advantages at the latter two gauging stations Sermide and Pontelagoscuro, i.e., for RMSE and CORR using kriging method is worse than the hydraulic statistic method. Besides, for BIAS and NSE using kriging method reveals no evident improvements.

Such a feature is highly spatially dependent, i.e., it depends on the distribution of gauging stations. This indicates that the quality of the densified water level time series is connected to the slope of the river course, as well as the river flow velocity. If we review the validation of the velocity model in Section 3.1, it is easy to find out that the weakness of the kriging method is closely linked to

the errors of the predicted velocities. At the fourth gauging station Sermide, the river flow velocity is severely biased. Besides, at the last gauging station Pontelagoscuro, the predicted velocities are very close to a constant. In such situations, where the velocities are relatively inaccurate and simulated with large rRMSE, the hydraulic statistic densification method outperforms the kriging densification method. Therefore, we can conclude that the hydraulic statistic densification method could have a better performance than kriging method when the predicted river velocities appear rough with large errors. This needs further experiments.

- (iv) Two densification methods show different characteristics for processing.

According to the graphical comparison made in Section 4.4, we can hold a view that these two densification methods have different priorities for processing. The kriging densification method will focus more on the contiguous interval of the predictor. Data with either larger temporal or spatial lags could be negligible for the prediction. This could make a better agreement of data structure for the kriging densification method against in situ data, where the highs and lows of water level are distinctly simulated and easy to distinguish. On the opposite, the hydraulic statistic densification method would rather deal with the entire time series without any preferences.

- (v) The problem that quite a few of the level peaks are not caught by any of the two densification methods, could be due to various reasons. One of the most likely reasons is that the altimetric missions miss some water level peaks. Instead, only the water levels at a preceding and a later time period with relatively lower water levels are observed. In such a case, no simulation of level peaks would be predicted, but only a general trend for this time fragment is predicted. For this reason, the results could not improve any further from a methodological standpoint, but only to adopt more satellite missions to fill the gaps.

Another possible could be that some level peaks occur only under particular conditions, such as extreme floods. Hence, such increments of water level are a random process, and there are no standard features to capture for the general prediction.

Alternatively, it is also possible that these peaks of water level are removed at the data snooping stage. If the data near the level peaks are few, these high-level peaks would have no references but only themselves with extremely high values. Hence, they might be considered as outliers compared to the surrounded lower heights. It is clear that the data snooping process takes the risk of losing information. In order to solve such a problem, we could improve the predictions from the methodological standpoint by modification of outlier identification. Note that removing outliers is always a significant process for geodetic or statistical works.

- (vi) When we look into Section 3.2, it is obvious that the first step of the kriging densification method is to transform altimetric time series of water level into residual data. We make a test: Applying either total time series or residual time series can have insignificant influences for the densification method.

We can find out that the kriging densification method only deals with the residual data so that a question arises, whether or not we apply the hydraulic statistic densification method with residual time series, the results could be better compared to processing total time series of water level. Because, when certain steps go wrong with residuals, the corresponding influences are logically smaller after restoring processing. Thus, we apply the residual time series to the hydraulic statistic densification method, too. More details are shown in Appendix B. From those results, we can see that applying either total signal or residual time series has an insignificant effect on the final densified time series.

5.2 Outlook

The future work is described in this section. To summarize, we list the following possibilities to improve the densification methods after our work:

- (i) We will apply the two densification methods in other rivers with more natural seasonal behaviours or more complicated river structures. In this thesis, the Po river is chosen. The tributaries of the Po river are not taken into consideration to simplify the calculation. Besides, the Po river is heavily influenced by artificial constructions, and its seasonal behaviour is relatively weak. Therefore, for the future work, we suggest to utilize other rivers with more distinct seasonalities to apply and compare these two densification methods. The comparison in such situation will be beneficial for a more conclusive comparison of densification methods. Furthermore, the altimetric time series from a more complex river, including its tributaries, are also suggested to incorporate. This could be a great help for a better understanding of the interaction and mutual effects between the main river course and its tributaries for the densification methods.
- (ii) To apply various river velocity models for the hydraulic statistic densification. Based on Section 3.1, we obtain a river flow velocity model based on river slope and river width. However, this model has errors to a certain degree, which affects the densification procedure. Therefore, other velocity models with different parameters are in request. For example, with the Gaukler-Manning-Strickler equation (Jirka, 2007), we can estimate the velocity differently:

$$V = kR^{\frac{2}{3}}S^{\frac{1}{2}}, \quad (5.1)$$

where, V is the velocity, R is the hydraulic radius, S is the river slope, and k is a constant Strickler coefficient representing the roughness of the course.

Besides, there are numerous other velocity models to be applied to the river provide a number of references. Each of them simulates the river velocity with different parameters, in other words, the different characteristics of the river. Under

such circumstances, we do not know which model could be better for the densification process. Thus, in the future, we recommend to apply and test more velocity models for the densification method. Priority for the selections is to apply the velocity model with more reliable and easily-accessible parameters.

- (iii) To apply various covariance model for the kriging densification. According to Section 3.2, for the kriging densification method, a simple product spatio-temporal covariance model was applied. However, many other covariance structures exist to model the spatial and temporal relationships according to De Cesare et al. (2001). Examples are:

- a) The product-sum model:

$$C_{st}(\tau_s, \tau_t) = k_1 C_s(\tau_s) C_t(\tau_t) + k_2 C_s(\tau_s) + k_3 C_t(\tau_t), \quad (5.2)$$

- b) The metric model:

$$C_{st}(\tau_s, \tau_t) = C(a^2|\tau_s|^2 + b^2|\tau_t|^2), \quad (5.3)$$

and

- c) The linear model:

$$C_{st}(\tau_s, \tau_t) = C_s(\tau_s) + C_t(\tau_t). \quad (5.4)$$

These spatio-temporal covariance models reflect different peculiarities of structures between time and space. Hence, in the future, it is recommended to apply and compare these various covariance models for the densification method. With its help, we may improve the performance of the kriging densification method, and acquire a general spatio-temporal covariance model which is especially suitable for densification purposes.

Bibliography

- Alsdorf, D. E., Rodríguez, E. and Lettenmaier, D. P. (2007), 'Measuring surface water from space', *Reviews of Geophysics* **45**(2).
- Baarda, W. (1968), 'A testing procedure for use in geodetic networks'.
- Birkett, C. (1995), The global remote sensing of lakes, wetlands and rivers for hydrological and climate research, in 'Geoscience and Remote Sensing Symposium, 1995. IGARSS'95. Quantitative Remote Sensing for Science and Applications', International', Vol. 3, IEEE, pp. 1979–1981.
- Birkinshaw, S. J., O'donnell, G., Moore, P., Kilsby, C., Fowler, H. and Berry, P. (2010), 'Using satellite altimetry data to augment flow estimation techniques on the mekong river', *Hydrological Processes* **24**(26), 3811–3825.
- Birkinshaw, S., Moore, P., Kilsby, C., O'donnell, G., Hardy, A. and Berry, P. (2014), 'Daily discharge estimation at ungauged river sites using remote sensing', *Hydrological Processes* **28**(3), 1043–1054.
- Bjerklie, D. M., Moller, D., Smith, L. C. and Dingman, S. L. (2005), 'Estimating discharge in rivers using remotely sensed hydraulic information', *Journal of Hydrology* **309**(1-4), 191–209.
- Boergens, E., Buhl, S., Dettmering, D., Klüppelberg, C. and Seitz, F. (2017), 'Combination of multi-mission altimetry data along the mekong river with spatio-temporal kriging', *Journal of Geodesy* **91**(5), 519–534.
- Bosch, W., Dettmering, D. and Schwatke, C. (2014), 'Multi-mission cross-calibration of satellite altimeters: Constructing a long-term data record for global and regional sea level change studies', *Remote Sensing* **6**(3), 2255–2281.
- Cressie, N. (1992), 'Statistics for spatial data', *Terra Nova* **4**(5), 613–617.
- Cressie, N. and Huang, H.-C. (1999), 'Classes of nonseparable, spatio-temporal stationary covariance functions', *Journal of the American Statistical Association* **94**(448), 1330–1339.
- Crétaux, J.-F. and Birkett, C. (2006), 'Lake studies from satellite radar altimetry', *Comptes Rendus Geoscience* **338**(14-15), 1098–1112.
- De Cesare, L., Myers, D. and Posa, D. (2001), 'Estimating and modeling space-time correlation structures', *Statistics & Probability Letters* **51**(1), 9–14.

- Dennis Jr, J. E. and Schnabel, R. B. (1996), *Numerical methods for unconstrained optimization and nonlinear equations*, Vol. 16, Siam.
- Jirka, G. H. (2007), *Einführung in die Hydromechanik*, KIT Scientific Publishing.
- Krige, D. (1952), 'A statistical analysis of some of the borehole values in the orange free state goldfield', *Journal of the Southern African Institute of Mining and Metallurgy* **53**(3), 47–64.
- McCuen, R. H., Knight, Z. and Cutter, A. G. (2006), 'Evaluation of the nash–sutcliffe efficiency index', *Journal of Hydrologic Engineering* **11**(6), 597–602.
- Michailovsky, C. I., Milzow, C. and Bauer-Gottwein, P. (2013), 'Assimilation of radar altimetry to a routing model of the brahmaputra river', *Water Resources Research* **49**(8), 4807–4816.
- Milzow, C., Krogh, P. E. and Bauer-Gottwein, P. (2011), 'Combining satellite radar altimetry, sar surface soil moisture and grace total storage changes for hydrological model calibration in a large poorly gauged catchment', *Hydrology and Earth System Sciences* **15**(6), 1729–1743.
- Nielsen, K., Stenseng, L., Andersen, O. B., Villadsen, H. and Knudsen, P. (2015), 'Validation of cryosat-2 sar mode based lake levels', *Remote Sensing of Environment* **171**, 162–170.
- Ponce, V. M. (1989), *Engineering hydrology: Principles and practices*, Vol. 640, Prentice Hall Englewood Cliffs, NJ.
- Soliman, S. S. and Hsue, S.-Z. (1992), 'Signal classification using statistical moments', *IEEE Transactions on Communications* **40**(5), 908–916.
- Tarpanelli, A., Barbetta, S., Brocca, L. and Moramarco, T. (2013), 'River discharge estimation by using altimetry data and simplified flood routing modeling', *Remote Sensing* **5**(9), 4145–4162.
- Tourian, M. J. (2012), Controls on satellite altimetry over inland water surfaces for hydrological purposes, Master's thesis.
- Tourian, M., Tarpanelli, A., Elmi, O., Qin, T., Brocca, L., Moramarco, T. and Sneeuw, N. (2016), 'Spatiotemporal densification of river water level time series by multimission satellite altimetry', *Water Resources Research* **52**(2), 1140–1159.
- Zhang, M. and Yuan, H. (1997), 'The pauta criterion and rejecting the abnormal value', *Journal of Zhengzhou University of Technology* **1**, 84–88.

Appendix A

Influence of the CryoSat-2 Mission for the Densification Process

Gauging Station		Piacenza	Cremona	Borgoforte	Sermide	Pontelago-scu-ro
BIAS [m]	NW	0.44	0.82	1.06	1.48	0.50
	W	0.45	1.09	0.99	1.51	0.47
STD [m]	NW	0.54	0.60	0.37	0.32	0.93
	W	0.53	0.65	0.32	0.28	0.91
RMSE [m]	NW	0.72	1.07	1.03	0.98	0.81
	W	0.72	1.07	1.01	1.00	0.81
CORR []	NW	0.50	0.57	0.65	0.64	0.67
	W	0.50	0.55	0.64	0.63	0.66
NSE []	NW	0.31	0.37	0.44	0.44	0.51
	W	0.30	0.39	0.45	0.44	0.52

Table A.1: Influence of CryoSat-2 mission for the hydraulic statistic densification method. (NW = data without CryoSat-2, W = data with CryoSat-2.)

The CryoSat-2 mission is excluded in our work for both densification methods to ensure the consistency. Additionally, to inspect the influence of CryoSat-2, we have made a test in the densification process. Two attempts – one with CryoSat-2, the other one not, have been carried out with the hydraulic statistic densification method. According to Table A.1, it can be seen that using or excluding CryoSat-2 altimetric data has no significant effects for the hydraulic statistic densification. This results indicates that removing CryoSat-2 has not much influence for our comparison between the two densification methods.

Appendix B

Applying the Hydraulic Statistic Densification Method with Residual Time Series

Gauging Station		Piacenza	Cremona	Borgoforte	Sermide	Pontelago- scuro
BIAS [m]	ALL	0.44	0.82	1.06	1.48	0.50
	RES	0.23	0.44	0.71	1.88	0.21
STD [m]	ALL	0.54	0.60	0.37	0.32	0.93
	RES	0.54	0.59	0.37	0.33	0.93
RMSE [m]	ALL	0.72	1.07	1.03	0.98	0.81
	RES	0.70	1.11	1.09	1.03	0.91
CORR []	ALL	0.50	0.57	0.65	0.64	0.67
	RES	0.47	0.56	0.63	0.62	0.61
NSE []	ALL	0.31	0.37	0.44	0.44	0.51
	RES	0.28	0.37	0.41	0.41	0.44

Table B.1: Influence of applying residual time series for the hydraulic statistic densification method. (ALL = applying total data, RES = applying residual data.)

In our work, the kriging densification method only deals with the residual data so that a question arises, whether or not we apply the hydraulic statistic densification method with residual time series, the results will be better as processing total water level time series. Because when certain steps go wrong with residuals, the corresponding influences are logically smaller after restoring processing. Thus, we apply the residual time series to the hydraulic statistic densification method, too. From Table B.1, we can see that except for BIAS, applying either total data or residual time series has an insignificant effect on the final densified time series.